Evaluating a fire smoke simulation algorithm in the National Air Quality Forecast Capability (NAQFC) by using multiple observation data sets during the Southeast Nexus (SENEX) field campaign

Li Pan [1,2*], HyunCheol Kim [1,2], Pius Lee [1], Rick Saylor [3], YouHua Tang [1,2], Daniel Tong [1,4], Barry Baker [1,5], Shobha Kondragunta [6], Chuanyu Xu [7], Mark G. Ruminski [6], Weiwei Chen [8], Jeff Mcqueen [9] and Ivanka Stajner [9]

[1] NOAA/OAR/Air Resources Laboratory, College Park, MD 20740, USA

[2] UMD/Cooperative Institute for Satellite Earth System Studies (CISESS), College Park, MD 20740, USA

[3] NOAA/OAR/ARL/Atmospheric Turbulence and Diffusion Division, Oak Ridge, TN 37830, USA

[4] GMU/CISESS, Fairfax, VA 22030, USA

[5] UMBC/CISESS, Baltimore, MD 21250, USA

[6] NOAA/NESDIS, College Park, MD 20740, USA

[7] I. M. Systems Group at NOAA, College Park, MD 20740, USA

[8] Northeast Institutes of Geography and Agroecology, Chinese Academy of Sciences, Changchun 130102, P. R. China

[9] NOAA/NCEP/Environmental Modeling Center, College Park, MD 20740, USA

Correspondence to: Li.Pan@noaa.gov

*Now at: *[NOAA/NCEP/EMC and I.M.S.G]*

Abstract

Multiple observation data sets: Interagency Monitoring of Protected Visual Environments (IMPROVE) network data, Automated Smoke Detection and Tracking Algorithm (ASDTA), Hazard Mapping System (HMS) smoke plume shapefiles and aircraft acetonitrile (CH_3CN) measurements from the NOAA Southeast Nexus (SENEX) field campaign are used to evaluate the HMS-BlueSky-SMOKE-CMAQ fire emissions and smoke plume prediction system. A similar configuration is used in the US National Air Quality Forecasting Capability (NAQFC). The system was found to capture most of the observed fire signals. Usage of HMS-detected fire hotspots and smoke plume information were valuable for both deriving fire emissions and forecast evaluation. This study also identified that the operational NAQFC did not include fire contributions through lateral boundary conditions resulting in significant simulation uncertainties. In this study we focused both on system evaluation and evaluation methods. We discussed how to use observational data correctly to retrieve fire signals and synergistically use multiple data sets. We also addressed the limitations of each of the observation data sets and evaluation methods.

Introduction

Wildfires and agricultural/prescribed burns are common in North America all year round, but predominantly occur during the spring and summer months (Wiedinmyer et al., 2006). These fires pose a significant risk to air quality and human health (Delfino et al., 2009; Rappold et al., 2011; Dreessen et al., 2016; Wotawa and Trainer 2000; Sapkota et al., 2005; Jaffe et al., 2013; Johnston et al., 2012). Since January 2015, smoke emissions from fires have been included in the National Air Quality Forecasting Capability (NAQFC) daily $PM_{2.5}$ operational forecast (Lee et al., 2017). The NAQFC fire simulation consists of: the NOAA National Environmental and Satellite Data and Information Service (NESDIS) Hazard Mapping System (HMS) fire detection algorithm, the U.S. Forest Service (USFS) BlueSky-fire emissions estimation algorithm, the U.S. EPA Sparse Matrix operator Kernel Emission (SMOKE) applied for fire plume

48   rise calculations, the NOAA National Weather Service (NWS) North American Multi-scale Model (NAM)

49   for meteorological prediction and the U.S. EPA Community Multi-scale Air Quality Model (CMAQ) for

50   chemical transport and transformation. In contrast to most anthropogenic emissions, smoke emissions

51   from fires are largely uncontrolled, transient and unpredictable. Consequently, it is a challenge for air

52   quality forecasting systems such as NAQFC to describe fire emissions and their impact on air quality

53   (Pavlovic et al., 2016; Lee et al., 2017; Huang et al., 2017).

54   Southeast Nexus (SENEX) was a NOAA field study conducted in the Southeast U.S. in June and July

55   2013 (Warneke et al., 2016). This field experiment investigated the interactions between natural and

56   anthropogenic emissions and their impact on air quality and climate change (Xu et al., 2016; Neuman et

57   al., 2016). In this work, the SENEX dataset was used to evaluate the HMS-BlueSky-SMOKE-CMAQ fire

58   simulations during the campaign period.

59   Two simulations were performed: one with and one without smoke emissions from fires during

60   the SENEX field campaign. Due to the large uncertainties in the estimates of fire emissions and smoke

61   simulations (Baker et al., 2016; Davis et al., 2015; Drury et al., 2014), the first step of the evaluation

62   focused on the fire signal capturing capability of the system. Differences between the two simulations

63   represented the impact of the smoke emissions from fires on the CMAQ model results. Observations from

64   various sources were utilized in this analysis: (i) ground observations (Interagency Monitoring of

65   Protected Visual Environments (IMPROVE)), (ii) satellite retrievals (Automated Smoke Detection and

66   Tracking Algorithm (ASDTA) and HMS smoke plume shape), and (iii) aircraft measurements (SENEX

67   campaign). Fire signals predicted by the modeling system were directly compared to these observations.

68   Several criteria have been used to rank efficacy of the observation systems for fire induced pollution

69   plumes.

Methodology

In this section the NAQFC fire modeling system used in the study was introduced. Uncertainties and limitations in the various modeling components of the system are discussed. Fig. 1 illustrates the schematics of the system. There are four processing steps:

HMS (Hazard Mapping System)

The NOAA NESDIS HMS is a fire smoke detection system based on satellite retrievals. At the time of this study, the satellite constellation used consists of 2 Geostationary Operational Environmental Satellite (GOES-10 and GOES-12) and 5 polar orbiting satellites: MODIS (Moderate-resolution Imaging Spectroradiometer)) instruments on NASA EOS -- Terra and Aqua satellites, and AVHRR (Advanced Very High Resolution Radiometer) instruments on NOAA 15/17/18 satellites. HMS detects wildland fire locations and analyzes their sizes, starting times and durations (Ruminski et al., 2008; Schroeder et al., 2008; Ruminski and Kondragunta 2006).

HMS first processes satellite data by using automated algorithms for each of the satellite platforms to detect fire locations (Justice et al., 2002; Giglio et al., 2003; Prins and Menzel 1992; Li et al., 2000), which is then manually analyzed by analysts to eliminate false detections and/or add missed fire hotspots. The size of the fire is represented by the number of detecting pixels corresponding to the nominal resolution of MODIS or AVHRR data. Fire starting times and durations are estimated from close inspection of the visible band satellite imagery. A bookkeeping file is generated at the end of this detection step, named "hms.txt" (Fig. 1). It includes all the thermal signal hotspots detected by the aforementioned 7 satellites. During the analyst quality control step, detected potential fire hotspots lacking visible smoke in the retrieval's HMS (RGB real-color) imagery are removed resulting in a reduced fire hotspot file called either "hmshysplit.prelim.txt" or "hmshysplit.txt" to be input into the BlueSky processing step.

93   In general, "hmshysplit.prelim.txt" and "hmshysplit.txt" are very similar, and "hmshysplit.txt" is

94 created later than "hmshysplit.prelim.txt" (Fig. 1). But the differences between "hmx.txt" and

95 "hmshysplit.txt" ("hmshysplit.prelim.txt") can be rather substantial. The reasons for differences are: 1)

96 many detected fires do not produce detectable smoke; 2) some fires/hotspots are detected only at night,

97 when smoke detection is not possible; 3) smoke emission HMS imagery is obscured by clouds thus not

98 detected by the analyst. Therefore, smoke emission occurrence provided by the HMS is a conservative

99 estimate of fire emissions.

100   By using multiple satellites the likelihood of detecting fires in HMS is robust. However, when the

101 fire geographical size is small the HMS detection accuracy dramatically decreases (Zhang et al., 2011; Hu

102 et al., 2016). Other limitations of the HMS fire detections include ineffective retrievals at nighttime and

103 under cloud cover.

104 BlueSky

105   BlueSky, developed by the USFS (US Forest Service), is a modeling framework to simulate smoke

106 impacts on regional air quality (Larkin et al., 2009; Strand et al., 2012). In this study, BlueSky acted as a

107 fire emission model to provide input for SMOKE (Herron-Thorpe et al., 2014; Baker et al., 2016). BlueSky

108 calculates fire emission based on HMS-derived locations (Fig. 1).

109   Fire geographical extent is reflected by the number of nearby fire pixels detected by satellites in

110 a 12-km CMAQ model grid. Fire pixels are converted to fire burning areas in BlueSky based on the

111 assumption that each fire pixel has a size of 1 km^2 and 10% of its area can be considered as burn-active

112 (Rolph et al., 2009). All fire pixels in a 12-km grid square are aggregated. BlueSky uses the following to

113 estimate biomass availability: fuel loading map is from the US National Fire Danger Rating System (NFDRS)

114 for the Conterminous US (CONUS) with the exception in western US where the HARDY set is used (Hardy

115 and Hardy 2007). BlueSky uses Emissions Production Model (EPM) (Sandberg and Peterson 1984), a simple

116 version of CONSUME, to calculate fuel actually burned -- the so-called consumption sums. Finally, EPM is

117 also used in BlueSky to calculate the fire emission hourly rate per grid-cell. BlueSky outputs CO, CO_2, CH_4,

118 non-methane hydrocarbons (NMHC), total PM, $PM_{2.5}$, PM_{10} and heat flux (Fig. 1).

119   BlueSky does not iteratively recalculate fire duration according to the modeled diminishing fuel

120 loading or the modeled fire behavior. In the aggregation process, when there is more than one HMS point

121 in a grid cell which have different durations, all points in that grid cell would be assigned the largest

122 duration in all points. For an example, if there were 3 HMS points that had durations of 10, 10 and 24

123 hours, the aggregation would include 3 points (representing 3 km^2) assigned with 24 hour duration to all

124 of the 3 HMS points.

125   HMS has no information about fuel loading. BlueSky uses a default fuel loading climatology over

126 the eastern US. BlueSky uses an idealized diurnal profile for fire emissions. Uncertainties in fire sizes, fuel

127 loading and fire emission rates lead to large uncertainties in wildland smoke emissions (Knorr et al., 2012;

128 Drury et al., 2014; Davis et al., 2015).

129 **SMOKE**

130   In SMOKE (Sparse Matrix Operator Kernel Emission), the BlueSky fire emissions data in a

131 longitude-latitude map projection are converted to CMAQ ready gridded emission files (Fig. 1). Fire smoke

132 plume rise is calculated using formulas by Briggs. The heat flux from BlueSky and NAM meteorological

133 state variables are used as input (Erbrink 1994). The Briggs' algorithm calculates plume top and plume

134 bottom, between plume top and bottom the emission fraction is calculated layer by layer assuming a

135 linear distribution of flux strength in atmospheric pressure. For model layers below the plume bottom the

136 emission fraction is assumed to be entirely in the smoldering condition as a function of the fire burning

137 area.

6

138   A speciation cross-reference map was adopted to match BlueSky chemical species to that in

139   CMAQ using the U.S. EPA Source Classification Codes (SCCs) for forest Wildfires

140   (https://ofmpub.epa.gov/sccsearch/docs/SCC-IntroToSCCs.pdf). The life-span of fire is based on the HMS

141   detected fire starting time and duration. During fire burning hours a constant emission rate is assumed.

142   This constant burn-rate has been shown to be a crude estimate (Saide et al., 2015; Alvarado et al., 2015).

143   Other uncertainties include plume rise (Sofiev et al., 2012; Urbanski et al., 2014; Achtemeier et al., 2011)

144   and fire-weather (fire influencing local weather).

CMAQ

146   The CMAQ version 4.7.1 was used. The CB05 gas phase chemical mechanism (Yarwood et al.,

147   2005) and the AERO5 aerosol module (Carlton et al., 2010) were chosen. Anthropogenic emissions were

148   based on the U.S. EPA 2005 National Emission Inventory (NEI) projected to 2013 (Pan et al., 2014),

149   Biogenic emissions (BEIS 3.14) were calculated in-line inside CMAQ.

Simulations

151   The NAM provided meteorology fields to drive CMAQ (Chai et al., 2013). NAM meteorology is

152   evaluated daily and results (BIAS and RMSE etc.) are posted on:

153   "http://www.emc.ncep.noaa.gov/mmb/mmbpll/mmbverif/". The simulation domain is shown in Fig. 1. It

154   includes two domains: (i) a 12-km domain covering the Continental U.S. (CONUS); and (ii) a 4km domain

155   covering the Southeast U. S. where the majority of SENEX measurements occurred. Lateral boundary

156   conditions (LBC) used in the smaller SENEX domain simulation were extracted from that from the CONUS

157   simulations. Four scenarios were simulated: CONUS with fire emissions, CONUS without fire emissions,

158   SENEX with fire emissions and SENEX without fire emissions.

159   There were several differences in system configuration between the NAQFC fire smoke

160   forecasting and the "with-fire" simulation in this study. For models, the BlueSky versions used in NAQFC

161   and that in this study are v3.5.1 and v2.5, respectively; CMAQ versions used in NAQFC and in this study

162   are v5.0.2 and v4.7.1, respectively. For simulations, current fire smoke forecasting in the NAQFC includes

163   two runs: the analysis and the forecast (Huang et al. 2019 (manuscript in preparation)). The analytical run

164   is a 24-hour retrospective simulation using yesterday's meteorology and fire emissions to provide initial

165   conditions for today's forecast. The forecasting run is a 48-hour predictive simulation using yesterday's

166   fire emissions, assuming fires with duration of more than 24 hours are projected as continued fires.. The

167   "with-fire" simulation in this study is exactly identical to the analysis run in NAQFC.

Evaluations

169   Carbon monoxide (CO) has a relatively long life time in the air and is emitted by biomass burning.

170   CO was used as a fire tracer in the prediction. The CO difference (ΔCO) between CMAQ simulations with

171   and without fire emissions was used as the indicator of fire influence. For additional observations

172   included: potassium (K) collected at the IMPROVE (Interagency Monitoring of Protected Visual

173   Environments) sites within the SENEX domain; acetonitrile (CH_3CN) measured from the SENEX campaign

174   flights; and fire plume shape detected by the HMS analysis as real fire signals. The enhancement in ΔCO

175   concentration due to fire was directly compared with those signals. At the same time, ΔAOD (Aerosol

176   Optical Depth) from CMAQ ("with-fire" simulated concentration minus that with "without-fire") was also

177   used as fire indicator when compared with smoke masks given by the ASDTA (Automated Smoke

178   Detection and Tracking Algorithm).

179   It is almost impossible to assess the uncertainty of each specific smoke physical process. In each

180   modeling step in HMS, BlueSky, SMOKE and CMAQ, the modeling system accrues uncertainties. Such

181   uncertainties were likely cumulative and might lead to larger error in succeeding components

182   (Wiedinmyer et al., 2011). For an example, heat flux from BlueSky influenced plume rise height in SMOKE

183   and consequently influenced plume transport in CMAQ. It is also noteworthy that when modeled ΔCO

184   was against measured K or CH_3CN, the objective was to search for enhancement signals resulting from

185   fires but not aiming to account for proportional concentration changes in the tracers in the event of a fire.

186   Attempting to account for CMAQ simulation uncertainties in surface ozone and particulate matter as a

187   function of smoke emissions from fires was difficult. Neither was it the objective of this study. Rather,

188   the purpose of this study is to focus on analyzing the capability of the HMS-BlueSky-SMOKE-CMAQ

189   modeling system to capture fire signals.

190   The SENEX campaign occurred in June and July and our model simulations were from June 10 to

191   July 20, 2013. Throughout the campaign all available observation datasets were used including ground-,

192   air- and satellite-based acquired data. Each dataset had its unique characteristics and linking them

193   together gave an overall evaluation. At the same time, in each dataset our evaluations included as many

194   as possible observed fire cases. Both well-predicted and poorly-predicted cases are presented to illustrate

195   potential reasons responsible for the modeling system's behavior.

Results and Discussions

196

Observed CO versus modeled CO in SENEX

197

198   Table 1 lists observed and modeled CO vertical profiles for the "with-fire" and "without-fire" cases

199   during the SENEX campaign. Observed CO concentrations between the surface and 7 km AGL (Altitude

200   above Ground Level) in the SENEX domain area remained greater than 100 ppb during all 40 days of the

201   campaign. The highest CO concentrations were measured closer to the surface. The maximum measured

202   CO concentration of 1277 ppb was observed during a flight on July 03 at an ASL (Altitude above Sea Level)

203   of 974 m. In this flight strong fire signals were observed but the fire simulation system missed those signals

204   as discussed below.

205   CO concentrations were underestimated by the model in almost all cases even when the model

206   captured CO contribution from fire emissions spatio-temporarily. Mean ΔCO in each height interval was

207   usually above 1.5 ppb but less than 2.0 ppb. Fig. 2a shows the contribution of total CO emissions from

208   fires which occurred inside the SENEX domain over the simulation period. The maximum CO emissions

209   contribution from fires was about 3% during the campaign. In most of those days fire emission

210   contributions in SENEX were less than 1%. The averaged contribution during those 40 days was 0.7%. Fig.

211   2b shows the contribution of CO flowing into the SENEX domain from its boundary caused by fire outside

212   the SENEX domain but inside the CONUS domain (Fig. 1). The averaged fire contribution to CO from

213   outside the SENEX domain was 0.67%. CO influenced by fire emission in June is greater than that in July.

214   During the field experiment the general lack of large fires made evaluation of modeled fire

215   signature difficult since it was easier to capture large fire signals than the smaller fires. We postulated that

216   a clear fire signal simulated in the HMS-BlueSky-SMOKE-CMAQ system could be indicated by ΔCO

217   significantly larger than its temporal averages resulted by fires originated from inside and/or outside the

218   SENEX domain. For an example, a clear fire signal between 500 m and 1000 m AGL was indicated by ΔCO

219   across those altitudes and when the concentration of ΔCO was above 2.0 ppb based on the campaign

220   duration averaged CO concentration of about 150 ppb as well as on within the SENEX domain and outside

221   of the SENEX domain fire contributions to CO (150*(0.007+0.0067) =2.0).

222   Figure 3 displays the simulated ΔCO extracted along SENEX flight path during the SENEX campaign.

223   The modeled concentration showed that the fire impacts on SENEX were not negligible despite a lack of

224   larger fire events as shown in Fig. 2a and 2b during the SENEX campaign period. That confirmed the

225   importance of evaluating the fire simulation system in an air quality model. Unless a model is able to

226   predict fire signals correctly it is useless for modelers to discuss fire effects on chemical composition of

227   the atmosphere. Details on how the model caught or missed or falsely predicted fire signals during the

228   SENEX campaign and a comparison of ΔCO versus CH_3CN will be discussed in the following discussion.

229   **IMPROVE**

230   The Interagency Monitoring of Protected Visual Environments (IMPROVE) is a long term air

231   visibility monitoring program initiated in 1985 (http://vista.cira.colostate.edu/Improve/data-page). It

232   provides 24-h integrated particulate matter (PM) speciation measurements every third day (Malm et al.,

233   2004; Eatough et al., 1996). The IMPROVE dataset was chosen for this analysis because it included K

234   (potassium), OC (organic carbon) and EC (elemental carbon), important fire tracers. IMPROVE monitors

235   are ground observation sites likely influenced by nearby fire sources.

236   There were 14 IMPROVE sites in the SENEX domain (Fig. 4). Potential fire signals were identified

237   by using CMAQ modeled ΔCO and IMPROVE observed K. However, in addition to fires K has multiple

238   sources such as soil, sea salt and industry. Co-incidentally fires should also produce enhanced EC and OC

239   concentrations, a fire signal should reflect above-average values for EC, OC, and K. EC, OC and K

240   observations that were 20% above their temporal averages during the SENEX campaign were used as a

241   predictor for fire event identification. Meanwhile, co-measured NO_3^- (nitrate) and SO_4^{2-} (sulfate)

242   concentrations are less than 1.5 times of their respective temporal averages for screening out data with

243   industrial influences. Lastly, a third predictor was employed so that concentrations of other soil

244   components besides K should be below their temporal average to eliminate conditions of spikes in K

245   concentration due to dust. With these three criteria the IMPROVE data was screened for fire events (See

246   Table 2).

247   Five fire events were observed at four IMPROVE sites. Table 2 lists measured EC, OC, NO_3^-, K, soil

248   and SO_4^{2-} concentrations (μg m^{-3}) and their ratios to averages. BC versus OC and K versus BC ratios were

249   also calculated and listed in Table 2 to illustrate the application of our criteria. It was found that except

250 for monitor BRIS, all other sites (COHU, MACA and GRSM) had BC/OC and K/BC ratios comparable to the

251 ratios of the same quantities due to biomass burning reported by other researchers (Reid et al., 2005;

252 DeBell et al., 2004). BRIS is a coastal site likely influenced by sea salt (Fig. 4).

253 For the four identified fire cases, ΔCO as a modeled fire tracer around the IMPROVE site was

254 plotted. Fire signals on June 21 at COHU and GRSM and on June 24 at MACA were reproduced in the "with

255 fire" model simulation. The June 24 MACA case was used as an example (see Fig. 4).On June 24, 2013,

256 detected fire spots were outside the SENEX domain, but SSW (south-southwest) wind blew smoke plumes

257 into the SENEX domain and affected modeled CO at MACA. Modeled ΔCO at MACA was 5 ppb.

258 Another IMPROVE site located upwind of MACA, CADI, was also potentially under the influence

259 of that fire event; however, data from CADI on June 24 did not indicate a fire influence, possibly due to

260 the frequency of IMPROVE sampling that eluded measurement or that the smoke plume was transported

261 above the surface in disagreement with what was modeled. Within the four fire cases identified by the

262 IMPROVE data during SENEX (Tab. 2), the model successfully captured three out of four events. The model

263 missed the fire signal on July 3 at MACA. The following section is dedicated to the July 3 SENEX flight.

264 **Plume Spatial Coverage**

265 HMS determines fire hotspot locations associated with smoke and upon incorporating the smoke

266 plume shape information from visible satellite images. HMS provides smoke plume shapefiles over much

267 of North America, which is a two-dimensional smoke plume spatial depiction collapsing all plume

268 stratifications to a satellite eye-view. For modeled plumes, we integrated modeled ΔCO by multiplying the

269 layer values with the corresponding CMAQ model layer thicknesses and air density to derive a simulated

270 smoke plume shape. HMS-derived smoke plume shape versus CMAQ predicted smoke plume shape was

271 then used to evaluate the fire simulation.

272   Figure of Merits in Space (FMS) (Rolph et al., 2009) is a statistic for spatial analysis and was

273   calculated as follows:

274
$$FMS = \frac{Area\_hms \ \cap \ Area\_cmaq}{Area\_hms \ \cup \ Area\_cmaq} \ X \ 100\%$$

275   Where Area_hms represent the area of grid cells influenced by fire emission over CONUS detected by

276   HMS and Area_cmaq represent the area of grid cells over CONUS identified by model prediction. In

277   general, a higher FMS value indicates a better agreement between the observed and modeled plume

278   shape (Rolph et al., 2009).

279   Figure 5 summarizes FMS during the SENEX campaign. Average FMS was 22% with its maximum

280   at 56% on July 6 and minimum at 1.2% on June 17 2013. Figure 6a exhibits HMS detected smoke plume

281   and CMAQ calculated smoke plume over CONUS on July 6. The FMS score was 56% meaning that the

282   modeled plume shape was consistent with that of HMS. However, HMS-BlueSky-Smoke emissions system

283   might have underestimated the intensive fire influence areas along the border of California and Nevada.

284   Subsequently, the model also under-predicted its associated influence in North Dakota, South Dakota,

285   Minnesota, Iowa and Wisconsin.

286   Figure 6b exhibits the worst case on June 17 2013 with a FMS score at 1.2%. Two reasons led to

287   this: (i) CMAQ missed the fire emissions from Canada. Those fire sources located outside the CONUS

288   modeling domain and our simulation system used a climatologically-based static LBC; Secondly on June

289   17, there were a lot of fire hotspots in the Southeastern U.S., i.e., in Louisiana, Arkansas and Mississippi

290   along the Mississippi River. Hotspots were detected but they lacked associated smoke in the

291   corresponding HMS imagery (Fig. 6c). This could be due to cloud blockage or to small agricultural debris

292   clearing, burns in under-bushes or prescribed burns. These conditions prevented the HMS from

293   identifying fires and hence emissions were not modeled for those sources.

294   It is noteworthy that the FMS evaluation contained uncertainties contributed from both modeled

295   and observed values. The calculated campaign duration and SENEX-wide averaged FMS was 22%. It is

296   significantly higher than that achieved by similar analyses done by HYSPLIT (Hybrid Single Particle

297   Lagrangian Integrated Trajectory) smoke forecasting for the fire season of 2007 (6.1% to 11.6%) (Rolph et

298   al., 2009). The primary reason is that due to retrieval latency and cycle-queuing problems in HMS, HMS

299   fire information is delayed by one day, which means that HMS today's list can only reflect yesterday's fire

300   information, so HYSPLIT smoke forecasting can only use yesterday's fire information. However, our model

301   simulation in this study was from a retrospective module using current day fire information. Such

302   discrepancies have been discussed by Huang et al. 2020 (*manuscript in preparation*). The secondary

303   reason is plume rise: although the HYSPLIT and CMAQ fire plume rise were both estimated by the Briggs'

304   equation, the HYSPLIT plume rise was limited to 75% of the mixed layer height (MLH) during daytime and

305   two times MLH at nighttime, whereas the CMAQ fire plume rise did not have these limitations.

306   **ASDTA**

307   The Automated Smoke Detection and Tracking Algorithm (ASDTA) is a combination of two data

308   sets: (1) the NOAA Geostationary satellite (G13) retrieves thermal enhancements aerosol optical depth

309   due to fires using visible channels and produces a product called GOES Aerosol/Smoke Product (GASP)

310   (Prados et al., 2007); and, (2) NOAA NESDIS HMS (Hazard Mapping System) fire smoke detection. First,

311   the observation of the increase in AOD near the fire is attributed to the specific HMS fire; AOD

312   values not associated with fires are dropped. Second, a pattern recognition scheme uses 30-

313   minutes geostationary satellite AOD images to tracks the transport of this smoke plume away

314   from the source. ASDTA provides the capability to determine whether the GASP is influenced by one or

315   multiple smoke plumes over a location at a certain time.

316   ASDTA, originally generate to provide operational support for verification of the NOAA HYSPLIT

317   dispersion model, predicts smoke plume direction and extension (Draxler and Hess 1998). These data are

318   also suitable for model performance evaluation in this study. For each simulation, modeled AOD was

319   calculated for each sensitivity test ("with-fire" or "without-fire") and ΔAOD is defined as the difference

320   obtained by subtracting AOD_without-fire from AOD_with-fire.

321   Figure 7a illustrates a GOES retrieved AOD (summed over from 10:00 am to 2:00 pm at local time)

322   contour plot that reflects influences by smoke plumes over the CONUS domain on June 14 2013. Figure

323   7b presents similar results, but for simulated ΔAOD (with-fire – without-fire). For further evaluation of

324   the HMS detected smoke plume shape Fig. 7c can be compared with Figs. 7a and 7b. Figure 7a shows

325   several regions under the influence of fires in: California, northwest Mexico, Kansas, Missouri, Oklahoma,

326   Arkansas, Texas and part of the Gulf of Mexico. In the northeastern USA, fire plumes occurred

327   occasionally. Those regions agreed relatively well with the shaded contours between Figs. 7a and 7c.

328   However, due to the lack of fire treatments in the CMAQ LBC, the simulation (Fig. 7b) missed smoke

329   influence on the northeast region of the CONUS domain. CMAQ also failed to simulate the fire influences

330   in the southwest region of the domain.

331   Similar plots for June 25 are shown in Figs. 7d, 7e and 7f for ASDTA, CMAQ and HMS, respectively.

332   The ASDTA (Fig. 7d) diagnosed an overestimation in fire influences in the south including Texas and the

333   Gulf of Mexico and an underestimation in the northeastern U.S. On the other hand, the model predicted

334   two strong fire signals clearly: near the border between Arizona and Mexico, and in Colorado (See Fig. 7e).

335   All the fire influenced areas in Fig. 7e were seen in the observations by HMS in Fig. 7f.

336   Comparing ASDTA plots and CMAQ ΔAOD plots (Fig. 7a vs 7b; Fig. 7d vs 7e), both similarities and

337   differences were found. Similarities were attributable to similar fire accounting and meteorology.

338   Differences were attributable to a number of reasons: HMS contains more fire hotspots than those used

15

339 by CMAQ due to domain size; only fires inside the CONUS were included in the CMAQ fire simulation and

340 LBCs did not vary to reproduce impacts of wildfires from outside of the domain.

SENEX

342   SENEX (Southeast Nexus) was a field campaign conducted by NOAA in cooperation with the US

343 EPA and the National Science Foundation in June and July 2013. Although SENEX was not specifically

344 designed for fire studies, its airborne measurements included $PM_{2.5}$ OC and EC, CO and acetonitrile

345 (CH_3CN). CH_3CN was chosen as a fire tracer since it is predominantly emitted from biomass burning

346 (Holzinger et al., 1999; Singh et al., 2012).

347   CH_3CN has a residence time in the atmosphere of around 6 months (Hamm and Warneck 1990)

348 and the reported CH_3CN background concentration is around 100 - 200 ppt (Singh et al., 2003). Measured

349 CH_3CN concentrations tend to increase with altitude (Singh et al., 2003; de Gouw et al., 2003), since

350 biomass burning plumes tend to ascend during long-range transport. During SENEX, measured CH_3CN

351 showed a similar pattern. Fire signals were identified through airborne measurements of CH_3CN when its

352 concentration exceeded the background; e.g., on July 3 2013, or when its concentration peak appeared

353 at high altitude; e.g., on June 16 2013 and July 10 2013.

354   CH_3CN airborne measurements were used to identify fire plumes at certain locations and heights

355 during SENEX. For model evaluation, fire locations and accurate meteorological wind fields are crucial to

356 interpret 2-D measurements such as IMPROVE, HMS and ASDTA. To verify a 3-D fire field, it is critical to

357 capture plume rise. However, it was extremely difficult to back out plume rise from the airborne

358 measurements. An additional uncertainty arose due to the difference in temporal resolutions of the data:

359 IMPROVE, HMS shapefiles and ASDTA were daily or hourly data, whereas airborne CH_3CN data were

360 measured at one-minute intervals.

361   Figure 8a shows a CMAQ simulated ΔCO vertical distribution along a flight transect on June 16

362   2013. This flight occurred during the weekend over and around power plants around Atlanta, GA. The

363   color along the flight path represents observed CH_3CN concentration in ppt. In Fig. 8a, the concentration

364   of ΔCO increased from surface to 5000 m, especially above 2000 m. Six CH_3CN concentration peaks were

365   observed when AGL was above 2500 m.

366   For CMAQ simulated ΔCO, five out of six fire signals detected by CH_3CN measured spikes were

367   captured where ΔCO concentrations were all above 3 ppb. Only one fire signal was missed by the model

368   at 18:30 UTC June 16 2013. The model simulation showed that long range transport (LRT) of smoke plumes

369   influenced airborne concentrations. Fire signals from the free troposphere subsided and influenced flight

370   measurements. High EC or OC or CO did not concur with high CH_3CN observation probably due to species

371   lifetime differences. HMS smoke plume did not show any hotspots or smoke plumes around Atlanta

372   suggesting that the sources of those observed fire signals were not from its vicinity.

373   A similar phenomenon was seen in SENEX flight 0710, which occurred during flight transects from

374   Tennessee to Tampa, FL. Figure 8b is a similar graph as Fig. 8a. Based on ΔCO concentrations, CMAQ

375   captured the July 10 case as fire signals were observed. Nonetheless, ΔCO may be over predicted at

376   around 19 UTC. The model exhibited a fire signal with ΔCO concentration of about 3 ppb near 6000 m

377   around 19 UTC, whereas measured CH_3CN was 120 ppt.

378   **SENEX flight on July 3**

379   Observations from IMPROVE, HMS and SENEX identified fire signals on July 3 2013. ASDTA

380   retrievals were not available. Those signals were missed by the model. In this section, all of the evaluation

381   methods addressed above were used to study potential causes of failure of the model to reproduce the

382   fire signals.

383   At the MACA IMPROVE site on July 3 2013, the wind direction at the surface was southeasterly,

384   with no fire hotspots (solid black circle) located upwind of MACA (Fig. 9a). Without any identified hotspots

385   upwind, the model missed fire signals observed at MACA on July 3 2013.

386   Flight #0703 was a night mission targeting power plants in Missouri and Arkansas. The flight path

387   is shown in Fig. 9b and is colored by measured CH_3CN concentrations. In order to highlight CH_3CH

388   concentrations above 400 ppt in the measurements, CH_3CN concentrations below 400 ppt were

389   represented by black dots. During the flight, 16 measurements of acetonitrile concentration above 400

390   ppt were observed and the maximum was 3227.9 ppt. These observations were located over

391   northwestern Tennessee and close to the borders of Kentucky, Illinois, Missouri and Arkansas. Except for

392   one observation, the flight ASL was between 500 m and 1000 m.

393   Enhancements of CO and OC were also measured concurrently with CH_3CN. Figures 9c and 9d

394   show scatter plots for CH_3CN versus CO and OC, respectively. Measured CH_3CN was highly correlated to

395   both measured CO and OC, with linear correlation coefficients (R^2) of 0.83 and 0.71, respectively. The

396    $\Delta CH_3CN/\Delta CO$ ratio is around 2.7 (ppt/ppb), which is consistent with findings of other measurements over

397   California in 2002 when a strong forest fire signal was intercepted by aircraft (de Gouw et al., 2003). The

398    $\Delta CH_3CN/\Delta OC$ ratio was around 6.85 (ppt/(mg m^{-3})), which is also in the range of biomass burning analyses

399   in MILAGRO (Megacity Initiative Local and Global Research Observations) (Aiken et al., 2010).

400   Figure 9e shows model simulated ΔCO with peaks at AGL below 3000 m. Fire signals have a

401   substantial influences on aircraft measurement at around 5 UTC. However, clear fire signals between 2

402   UTC and 3 UTC were observed based on prior CH_3CN analysis. The model either predicted insufficient fire

403   emission influences or missed it. FMS score on July 3 was 30%. Figure 9f shows that CMAQ did not predict

404   plumes where the HMS plume analysis exhibited several dense smoke plumes. As NOAA Smoke Text

405   Product (http://www.ssd.noaa.gov/PS/FIRE/DATA/SMOKE) described on its July 03 0501 UTC report: a

18

406   smaller very dense patch of remnant smoke, analyzed earlier the same day over southern Missouri, drifted

407   southward into Arkansas."

408   The reasons the model missed these fire observations are not clear. Figures 10, 11a and 11b

409   suggest a few clues. Figure 10 is a backward trajectory analysis plot for the observations obtained during

410   the SENEX flight on July 3 with observed CH_3CN concentrations above 400 ppt. Both transect and passing

411   altitude of the air parcels clearly showed those measurements were most likely influenced by the nearby

412   pollution sources. Figure 11a illustrates the locations of fire used in the CMAQ simulation. It is noted that

413   hmshysplit.txt is input into BlueSky after HMS quality control (Fig. 1). There were several hotspots around

414   the region where the IMPROVE site MACA was located and where the SENEX flight overpassed. Our fire

415   simulation system might have underestimated smoke emissions from those fires. Another explanation

416   can be seen from Fig. 11b, which illustrated hotspots in hmx.txt. In hmx.txt, every detected fire spots by

417   HMS before quality control are shown. Comparing Fig. 11a with 11b, there are clusters of fire spots in the

418   central U. S. especially in West Tennessee. However, those spots were removed during the HMS quality

419   control process because there were no associated smoke plumes visible. In most cases, those fires were

420   believed to be small sized fires such as from agriculture fires or prescribed burns. For this particular case,

421   there seem to have been thin clouds overhead and thicker clouds in the vicinity,

422   (http://inventory.ssec.wisc.edu/inventory/image.php?sat=GOES-13&date=2013-07

423   03&time=16:02&type=Imager&band=1&thefilename=goes13.2013.184.160147.INDX&coverage=CONUS

424   &count=1&offsettz=0), so it would be hard to differentiate smoke from clouds by satellite observations.

CONCLUSIONS

426   In support of the NOAA SENEX field experiment in June-July 2013, simulations were conducted

427   including smoke emissions from fires. In this study, a system accounting for fire emissions in a chemical

428   transport model is described, including a satellite fire detecting system (HMS), a fire emission calculation

429   model (BlueSky), a pre-processing of fire emissions (SMOKE), and simulation over the SENEX domain by

430   CMAQ. The focus of this work is to evaluate the system's capability to capture fire signals identified by

431   multiple observation data sets. These data sets included IMPROVE ground station observations, satellite

432   observations (HMS plume shapefile and ASDTA) and airborne measurements from the SENEX campaign.

433   For the IMPROVE data, potential fire signals were identified by measured potassium

434   concentrations in $PM_{2.5}$. Fire identifications in CMAQ rely on predicted ΔCO, the difference between

435   simulations with and without fire emissions. Three out of four observed fire signals were captured by the

436   CMAQ simulations. For HMS smoke plume shapefiles that were manually plotted by analysts to represent

437   the regions impacted by smoke, we used FMS to calculate the percentage of its overlap with CMAQ

438   predicted smoke plumes. FMS averaged 22% over forty days of the SENEX campaign. In terms of fire

439   smoke impacts on ΔAOD, both ASDTA and CMAQ showed patterns that were compared to HMS plume

440   shapefile. In terms of measured CH_3CN, a biomass burning plume tracer, both SENEX aircraft in-flight

441   measurements and CMAQ simulations captured signatures of long range transport of fire emissions from

442   elsewhere in the CONUS domain.

443   Generally, using HMS-detected fire hotspots and smoke data was useful for predictions of fire

444   impacts and their evaluation. The HMS-BlueSky-SMOKE-CMAQ fire simulation system, which is also used

445   in NAQFC, was able to capture most of the fire signals detected by multiple observations. However, the

446   system failed to identify fire cases on June 17 and July 3 2013 -- thereby demonstrating two problems

447   with the simulation system. One identified problem was the lack of a dynamical fire LBC bounding the

448   CONUS domain to represent the inflow of strong fire signals originating from outside the simulation

449   domain. Secondly, the HMS quality control procedure eliminated fire hotspots that were not associated

450   with visible smoke plumes leading to an underestimation.

451   We were keen on understanding and quantifying the various uncertainties and observational

452   constraints of this study therefore the following rules of thumb were observed: (1) a holistic evaluation

453   approach was adopted so that the fire smoke algorithm was interpreted as a single entity to avoid

454   deadlock due to over-interpretation of uncertainty of the single component in the system; (2) analysis

455   conclusion applicable to the entire simulation period was drawn so that the episodic characteristics of the

456   cases embedded in the simulation were averaged and generalized. This new methodology may benefit

457   NAQFC; (3) we took advantage of the multiple perspectives of the observation systems that offered a wide

458   spectrum of temporal and spatial variabilities intrinsic to the systems; (4) we were intentionally

459   conservative in discarding data so that we maximized the sampling pool for statistical analysis and avoided

460   unwittingly discarding poorly simulated cases, good outliers, and weak but accurate signals.

461   Quantitative evaluation of fire emissions and their subsequent influences on ozone and

462   particulate matter in this fire and smoke prediction system is challenging. Future work includes applying

463   these findings to the NAQFC and improving the NAQFC system's capabilities to simulate fires accurately.

464   **Code Availability**

465   The source code used in this study is available online at

466   http://www.nco.ncep.noaa.gov/pmb/codes/nwprod/cmaq.v5.0.2.

467   **Acknowledgements & disclaimer**

Figures:

473

474 Figure 1, schematics of fire emission and smoke plume simulation system used: Data-feed and/or
475 modeling of physical and chemical processes were handled largely sequentially from top to bottom and
476 from left to right; The right hand four vertical boxes depict the submodel names: NESDIS Hazard Mapping
477 System (HMS) for wild fire hot spot detection; US Forest Service's BlueSky for fuel type and loading
478 parameterization; and US EPA's Sparse Matrix Operator Kernel (SMOKE) to handle emission
479 characterization; and lastly the Community Multiple-scale Air Quality model (CMAQ) was applied to
480 simulate the transformation, transport and depositions of the atmospheric constituents. The "SENEX" in-
481 set framed by red emboldened lines was the domain for this study.

482 Figure 2, in 4km SENEX domain, (a): the contribution (%) of CO emission from fires occurred inside the
483 SENEX domain; (b): the contribution (%) of CO flux flowing into the SENEX domain from its boundary
484 caused by fires burning outside the SENEX domain but inside the CONUS domain.

485 Figure 3, CMAQ simulated ΔCO (ppb): i.e., the CO concentration difference between CMAQ simulation
486 with and without fire emissions, extracted along the overall SENEX flight paths during the SENEX campaign
487 between June 10 and July 20 2013.

488 Figure 4, simulated ΔCO (>2.0 ppb) in the SENEX domain on June 24 2013 at 20:00 UTC overlaid with 2 m
489 wind arrows with a 10 m s^{-1} reference arrow shown in the bottom right. The solid black circle is detected
490 fire hotspots by HMS. The solid triangles labeled with station code represents IMPROVE sites used in
491 model verification calculations.

492 Figure 5, FMS (Figure of Merits in Space) (%) from June 11 to July 19 in 2013 during the SENEX campaign.

493 Figure 6, Daily HMS observed plume shape versus CMAQ predicted daily averaged plume shape on (a):
494 July 6 2013; (b): June 17 2013; The light blue shading represents modeled plume shape (defined as total
495 column ΔCO) and the thin dash line and emboldened green lines encircle areas representing HMS-derived
496 light and strong influenced plume shape, respectively. (c): HMS observed fire hotspots (red) and plume
497 shapes (white) (http://ready.arl.noaa.gov/data/archives/fires/national/arcweb) on June 17, 2013.

498 Figures 7, GOES detected AOD influenced by fires using ASDTA diagnose method (summed over from
499 10:00 am to 2:00 pm local time). Color-shaded region represents the fire-smoke influenced areas and the
500 color denotes the magnitude of the retrieved AOD on (a): June 14 2013; (d): June 25 2013; simulated
501 ΔAOD (withfire – nofire) calculated by CMAQ on (b): June 14 2013; (e): June 25 2013; HMS observed fire
502 hotspots (red) and plume shapes (white) on (c): June 14 2013; (f): June 25 2013.

503 Figure 8, vertical distributions of CMAQ simulated ΔCO (ppb) shown along a flight transect on (a): June 16
504 2013; (b): July 10 2013; the x-axis label is UTC (hour) and y-axis label is AGL (m). Two color bars represent
505 observed CH3CN concentration (filled square dots and rectangle bar in ppt) and simulated ΔCO
506 concentration (backdrop color shading and fan bar in ppb), respectively.

507 Figure 9, plots for July 3 2013 case, (a): IMPROVE; (b): the flight path of SENEX #0703 colored by measured
508 CH$_3$CN concentration (ppt); (c): CH$_3$CN (ppt) vs CO (ppb); (d): CH$_3$CN (ppt) vs AMS_Org (mg m^{-3}); (e): CMAQ

509 simulated ΔCO vertical distributions along a flight transect; (f): HMS observed plume shape versus CMAQ
510 prediction.

511 Figure 10, a backward trajectory analysis for CH_3CN concentration greater than 400 ppt measured along
512 a SENEX flight on July 03 in: (upper) aerial, and (lower) time vertical cross-sections.

513 Figure 11, detected fire hotspots on July 03 2013 as daily composite (a): hmxhysplit.txt; (b): hmx.txt.

514

515

516

517

518

519

520

521

522

523
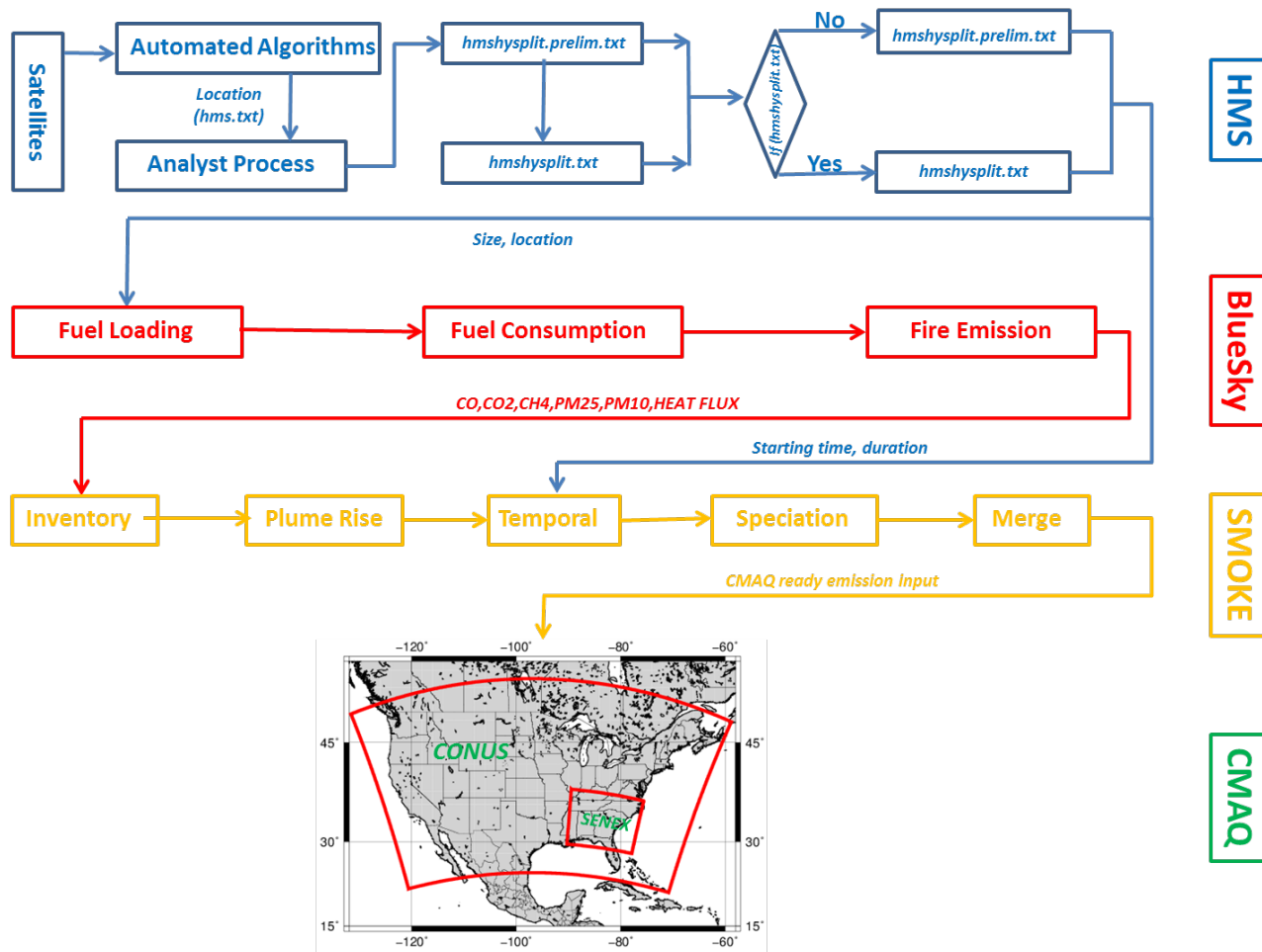
524

Figure 1: schematics of fire emission and smoke plume simulation system used: Data-feed and/or modeling of physical and chemical processes were handled largely sequentially from top to bottom and from left to right; The right hand four vertical boxes depict the submodel names: NESDIS Hazard Mapping System (HMS) for wild fire hot spot detection; US Forest Service's BlueSky for fuel type and loading parameterization; and US EPA's Sparse Matrix Operator Kernel (SMOKE) to handle emission characterization; and lastly the Community Multiple-scale Air Quality model (CMAQ) was applied to simulate the transformation, transport and depositions of the atmospheric constituents. The "SENEX" in-set framed by red emboldened lines was the domain for this study.

533

534

535
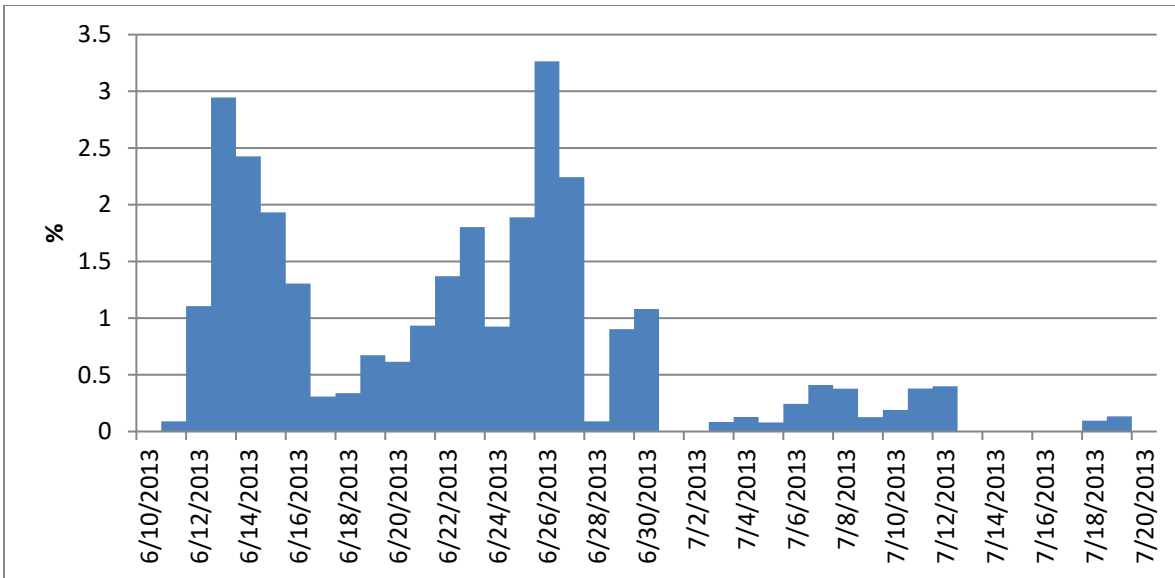
Figure 2a: the contribution (%) of CO emission from fires occurred inside the SENEX domain.

537
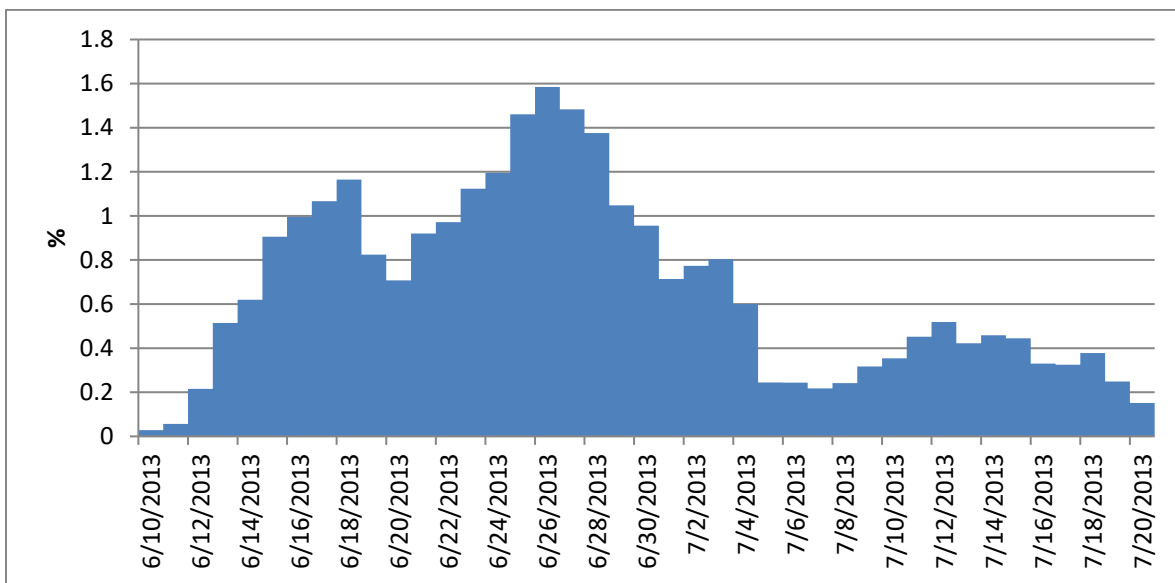
Figure 2b: the contribution (%) of CO flux flowing into the SENEX domain from its boundary caused by fires burning outside the SENEX domain but inside the CONUS domain.

540

541
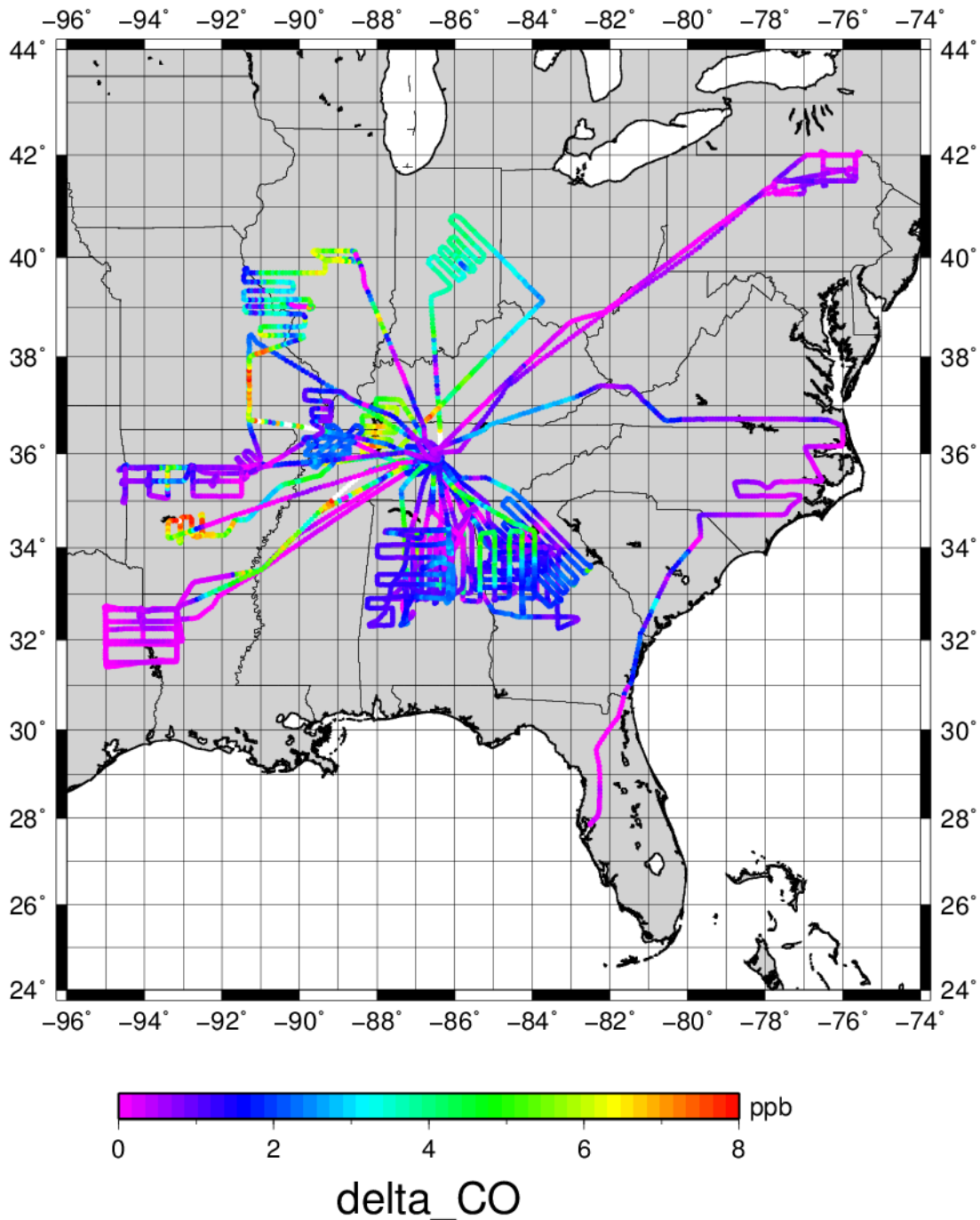
542

Figure 3: CMAQ simulated ΔCO (ppb): i.e., the CO concentration difference between CMAQ simulation
with and without fire emissions, extracted along the overall SENEX flight paths during the SENEX
campaign between June 10 and July 20 2013.
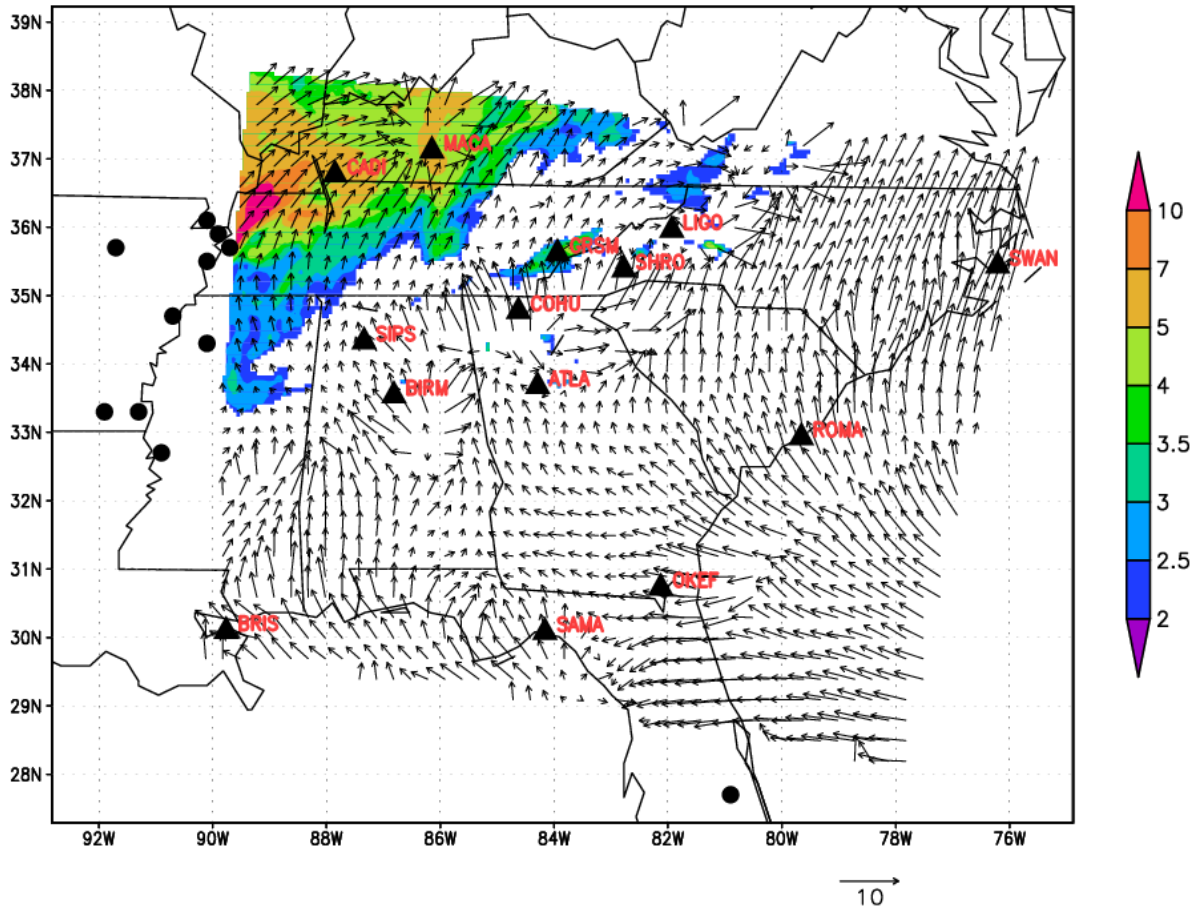
546

Figure 4: simulated ΔCO (>2.0 ppb) in the SENEX domain on June 24 2013 at 20:00 UTC overlaid with 2 m wind arrows with a 10 m s^{-1} reference arrow shown in the bottom right. The solid black circle is detected fire hotspots by HMS. The solid triangles labeled with station code represents IMPROVE sites used in model verification calculations.

551

552

553

554

555

556

557

558

559

560
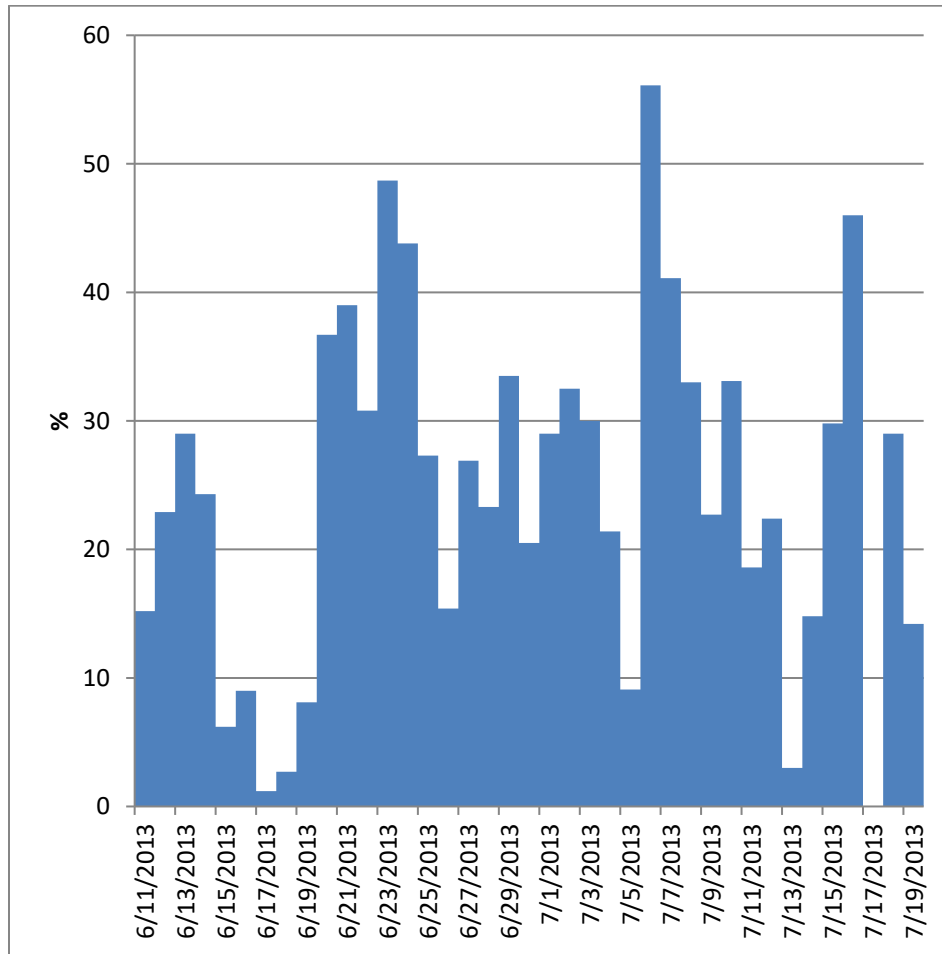
561

Figure 5: FMS (Figure of Merits in Space) (%) from June 11 to July 19 in 2013 during the SENEX campaign.

562
563

564

565

566

567

568

569

570

571

572

573
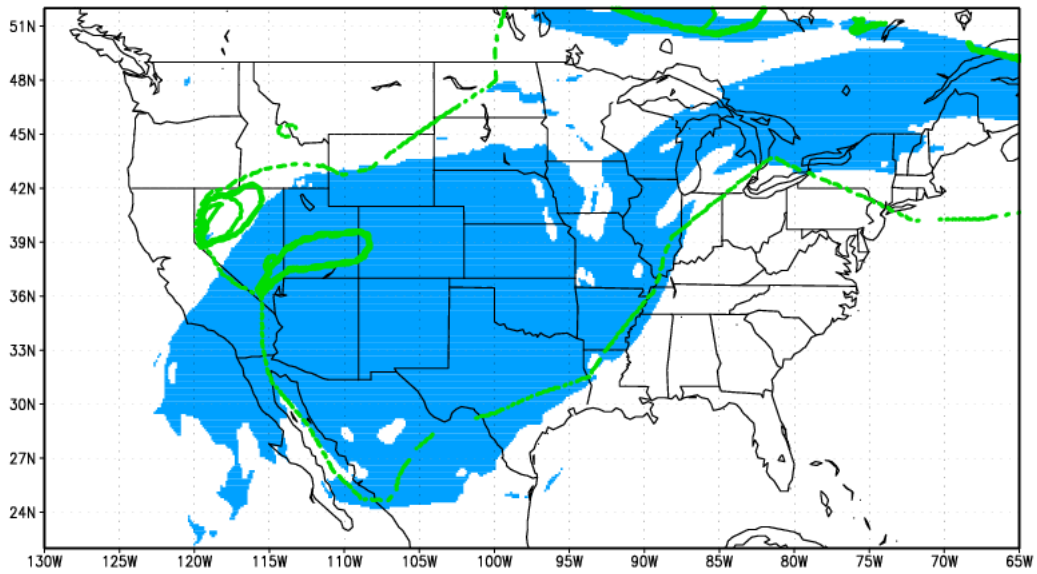
Figure 6a: Daily HMS observed plume shape versus CMAQ predicted daily averaged plume shape on July 6 2013; The light blue shading represents modeled plume shape (defined as total column ΔCO) and the thin dash line and emboldened green lines encircle areas representing HMS-derived light and strong influenced plume shape, respectively.

578
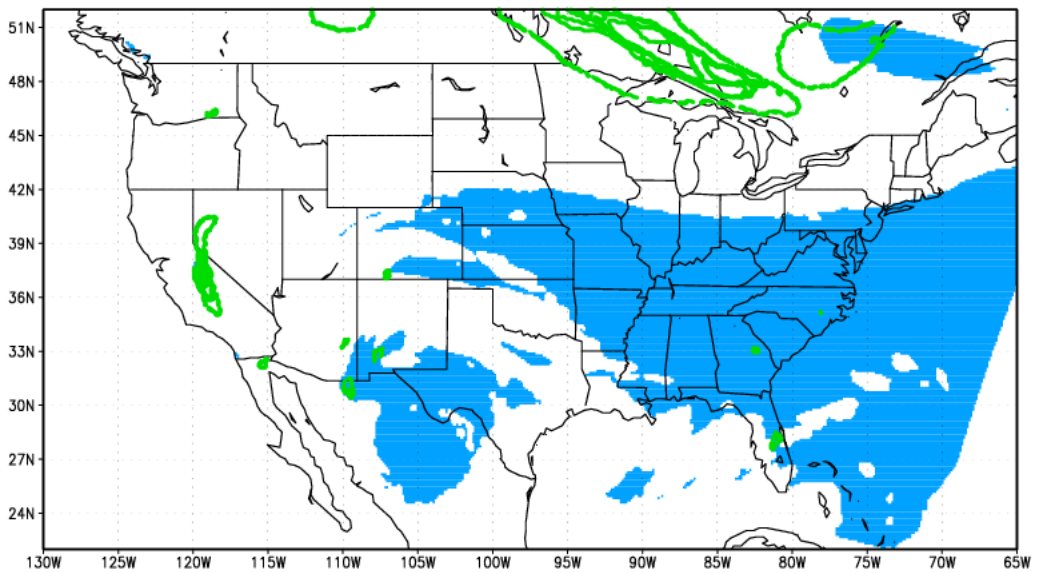
Figure 6b: same as Figure 6a but for June 17 2013.

580

29
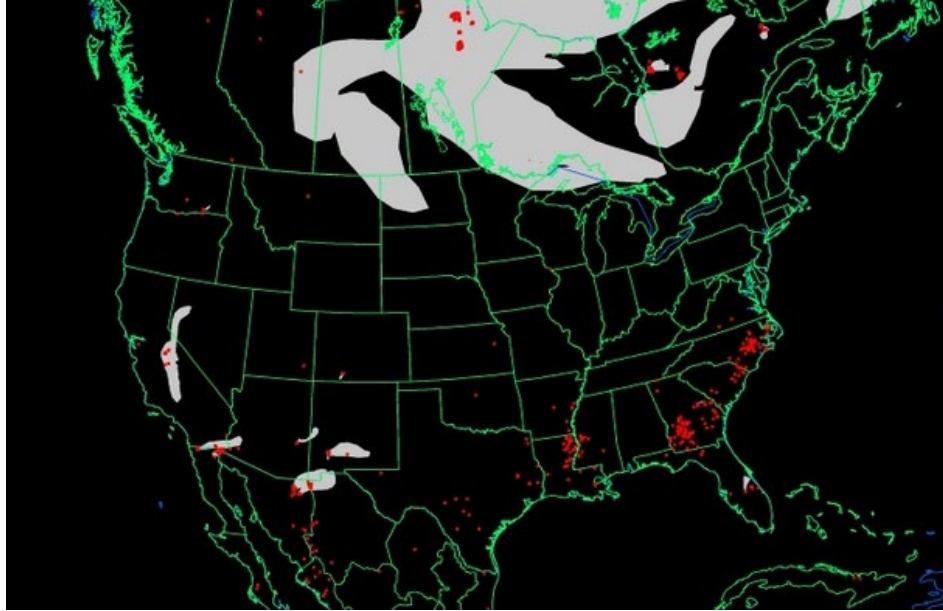
Figure 6c: HMS detected fire hotspots (red) and smoke plume shapes (white) on June 17 2013
(analysis day: 20130717, map generated: around 1100 GMT).
(http://ready.arl.noaa.gov/data/archives/fires/national/arcweb).
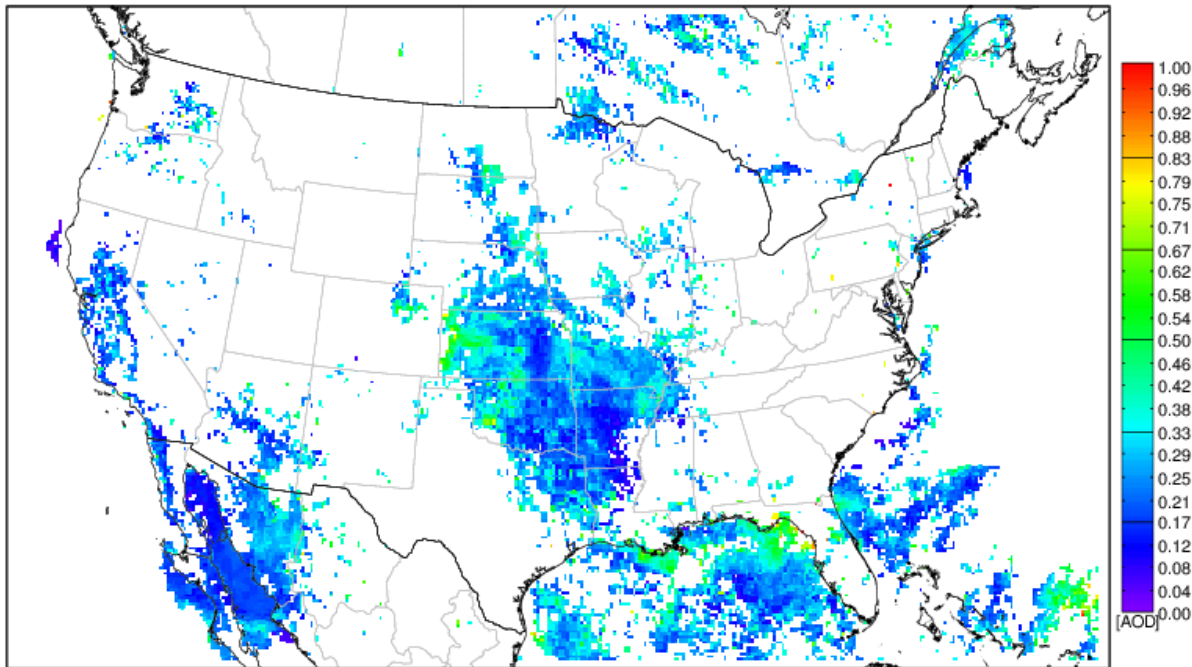
Figure 7a: GOES detected AOD influenced by fires using ASDTA diagnose method on June 14 2013

(summed over from 10:00 am to 2:00 pm local time). Color-shaded region represents the fire-smoke

influenced areas and the color denotes the magnitude of the retrieved AOD.

30

589
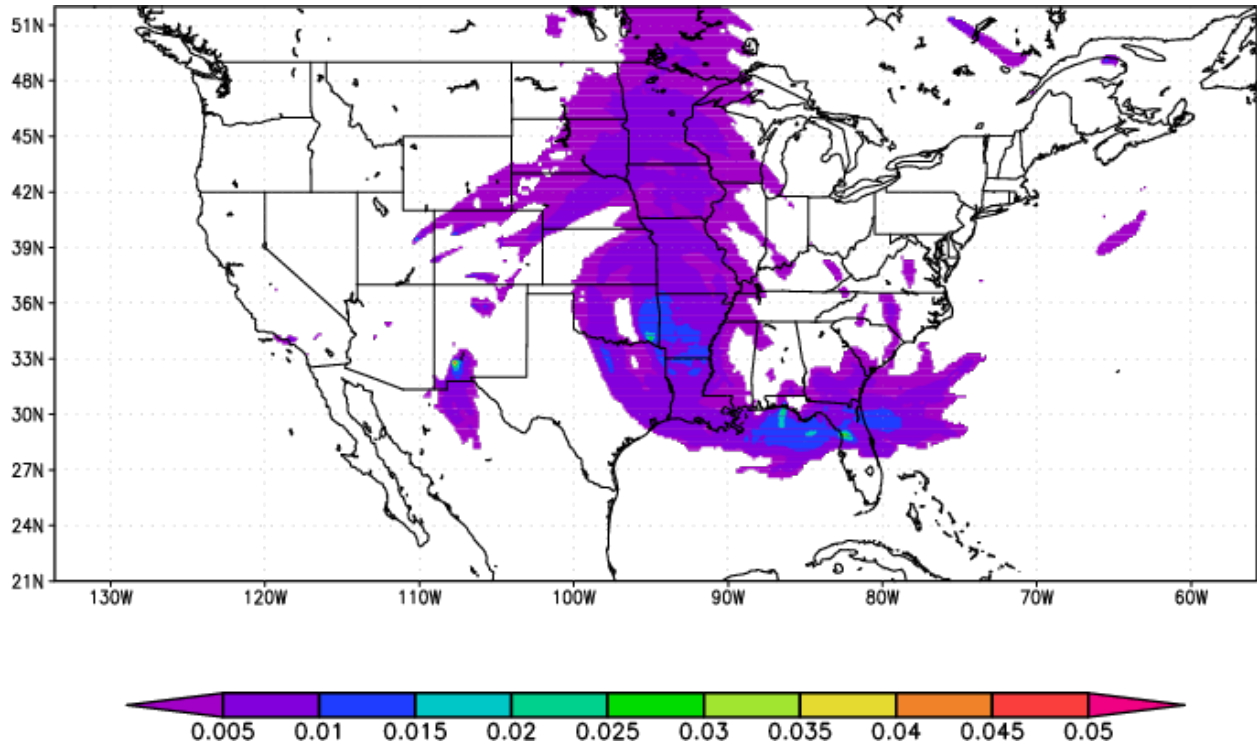
590   **Figure 7b: simulated ΔAOD (with-fire − without-fire) calculated in CMAQ on June 14 2013.**

591
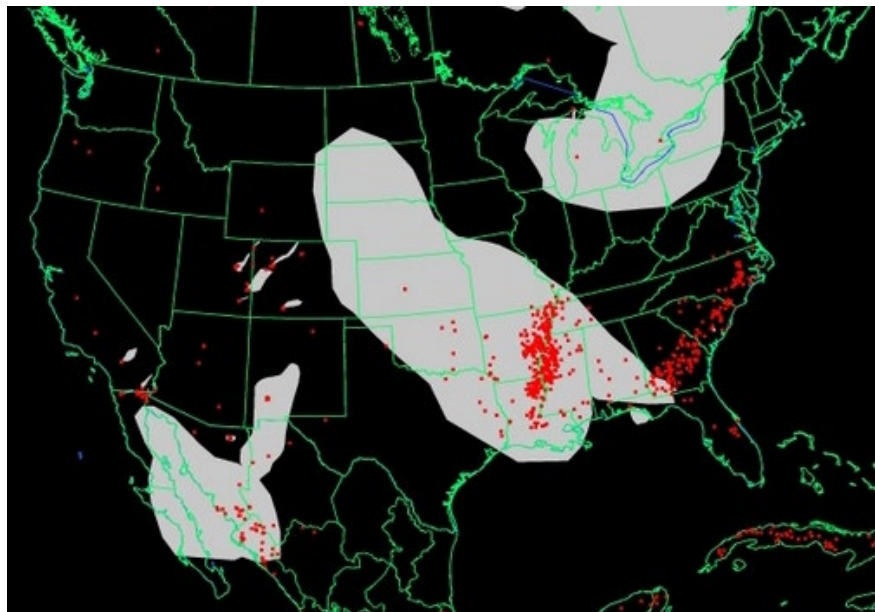
592   **Figure 7c: same as Figure 6c but for June 14 2013.**

593

594

595
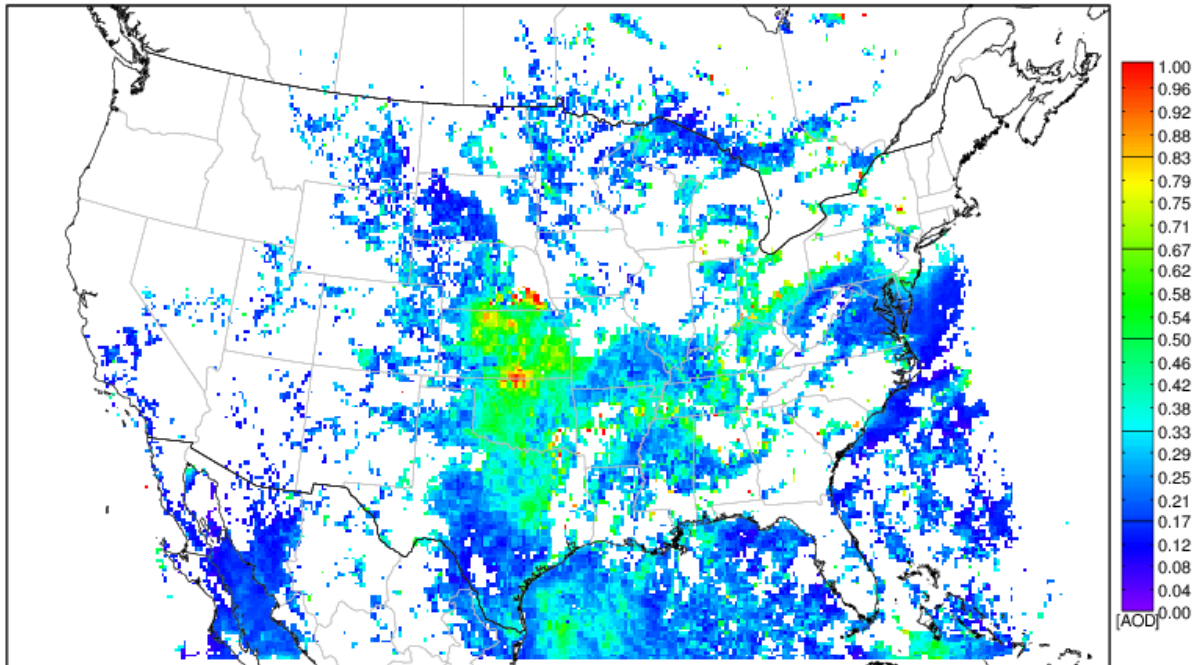
Figure 7d: same as Figure 7a but for June 25 2013.

597

598
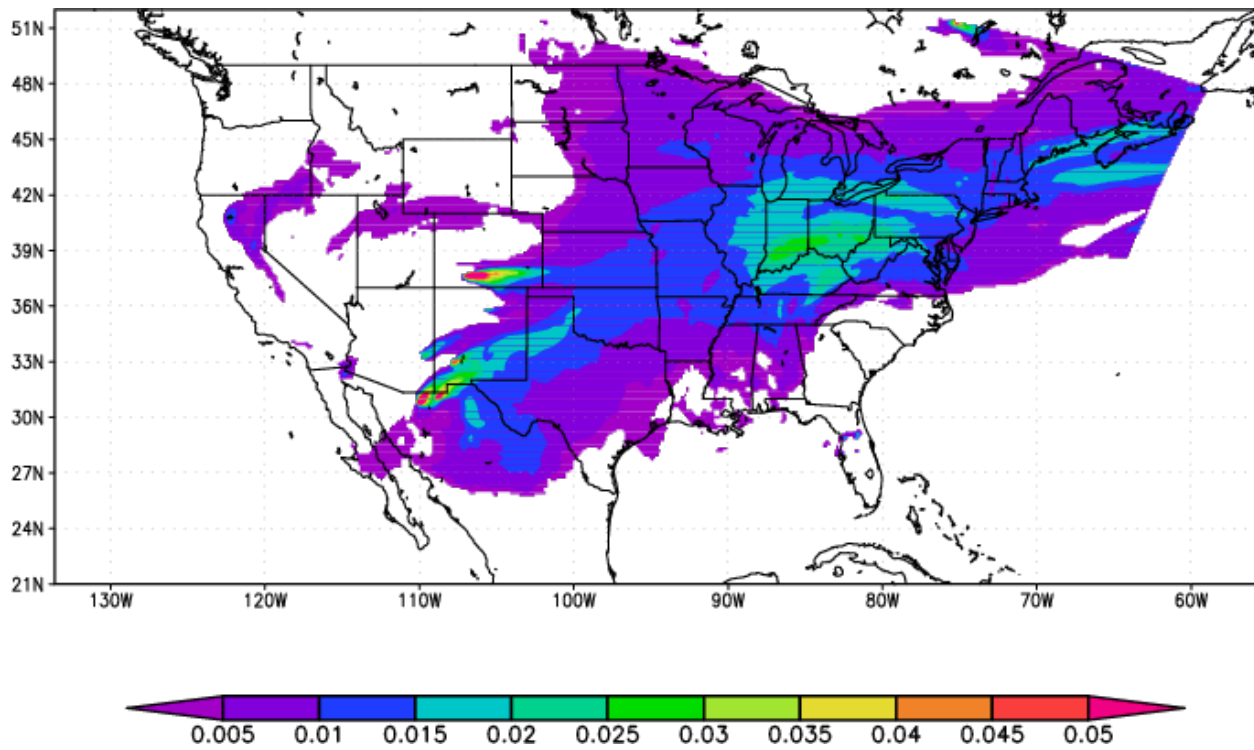
Figure 7e: same as Figure 7b but for June 25 2013.

32

600

602

603

604
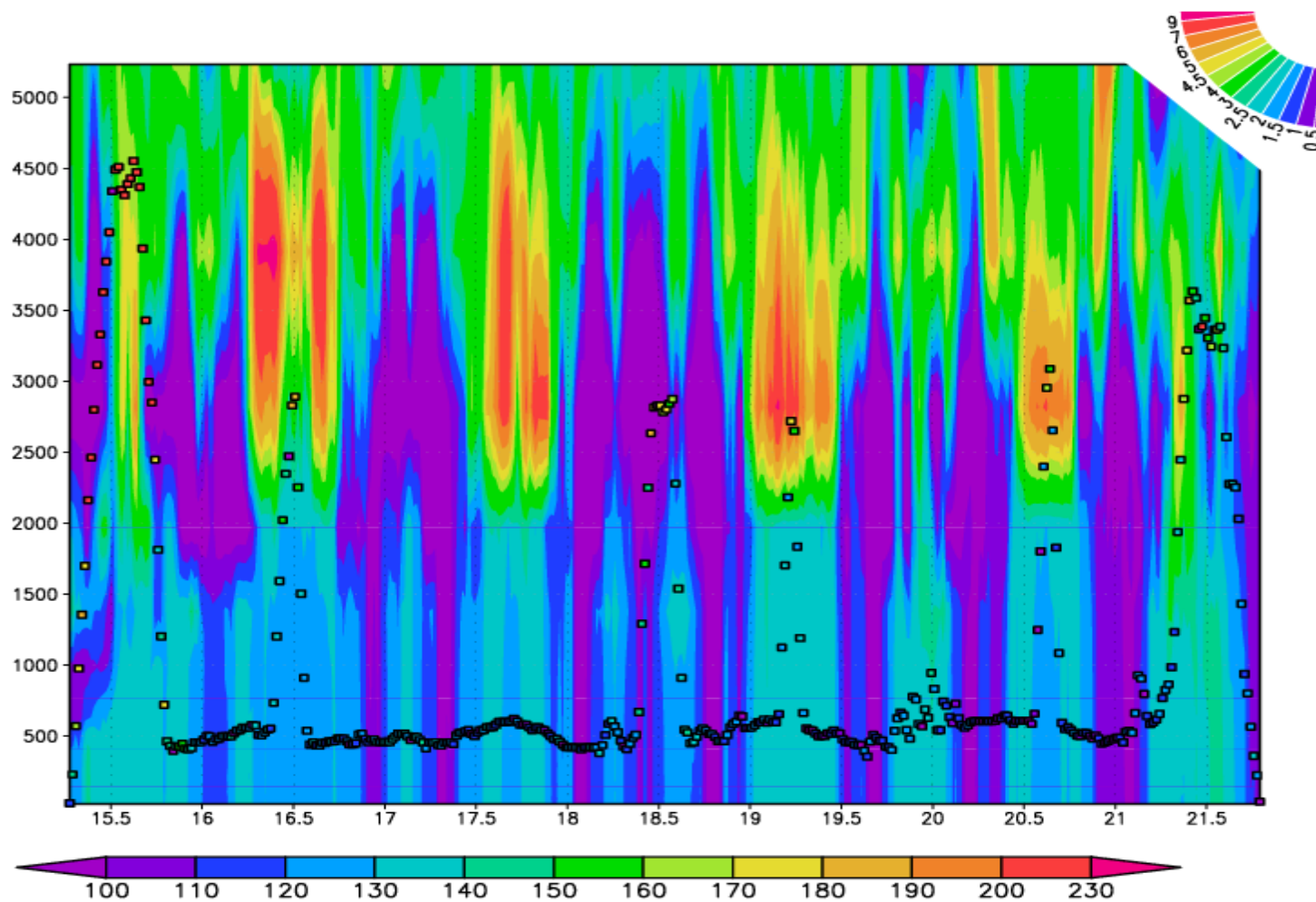
Figure 8a: vertical distributions of CMAQ simulated ΔCO (ppb) shown along a flight transect on June 16 2013. The x-axis label is UTC (hour) and y-axis label is AGL (m). Two color bars represent observed CH_3CN concentration (filled square dots and rectangle bar in ppt) and simulated ΔCO concentration (backdrop color shading and fan bar in ppb), respectively.
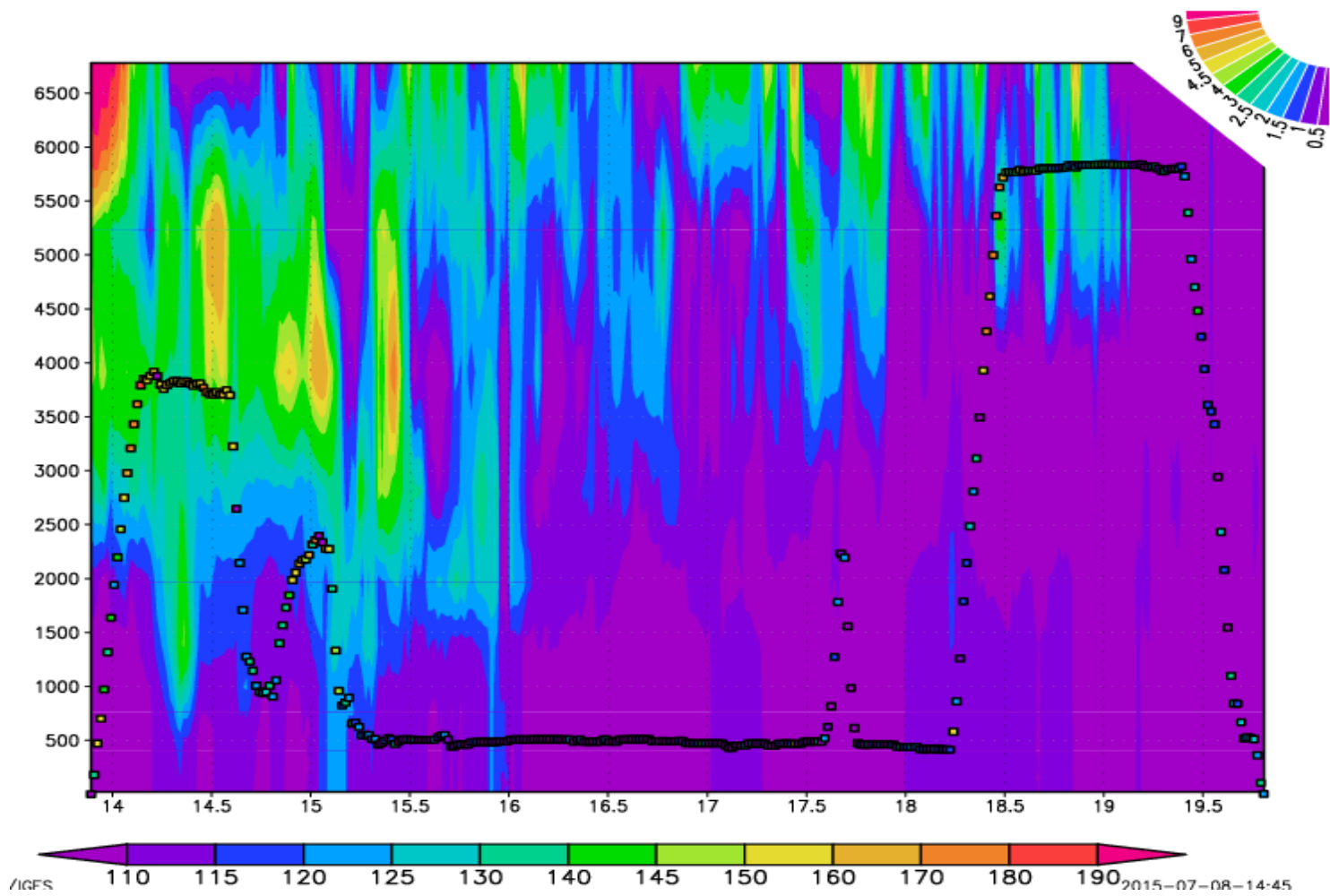
608

609

610   **Figure 8b: same as Figure 8a but for July 10 2013.**

611
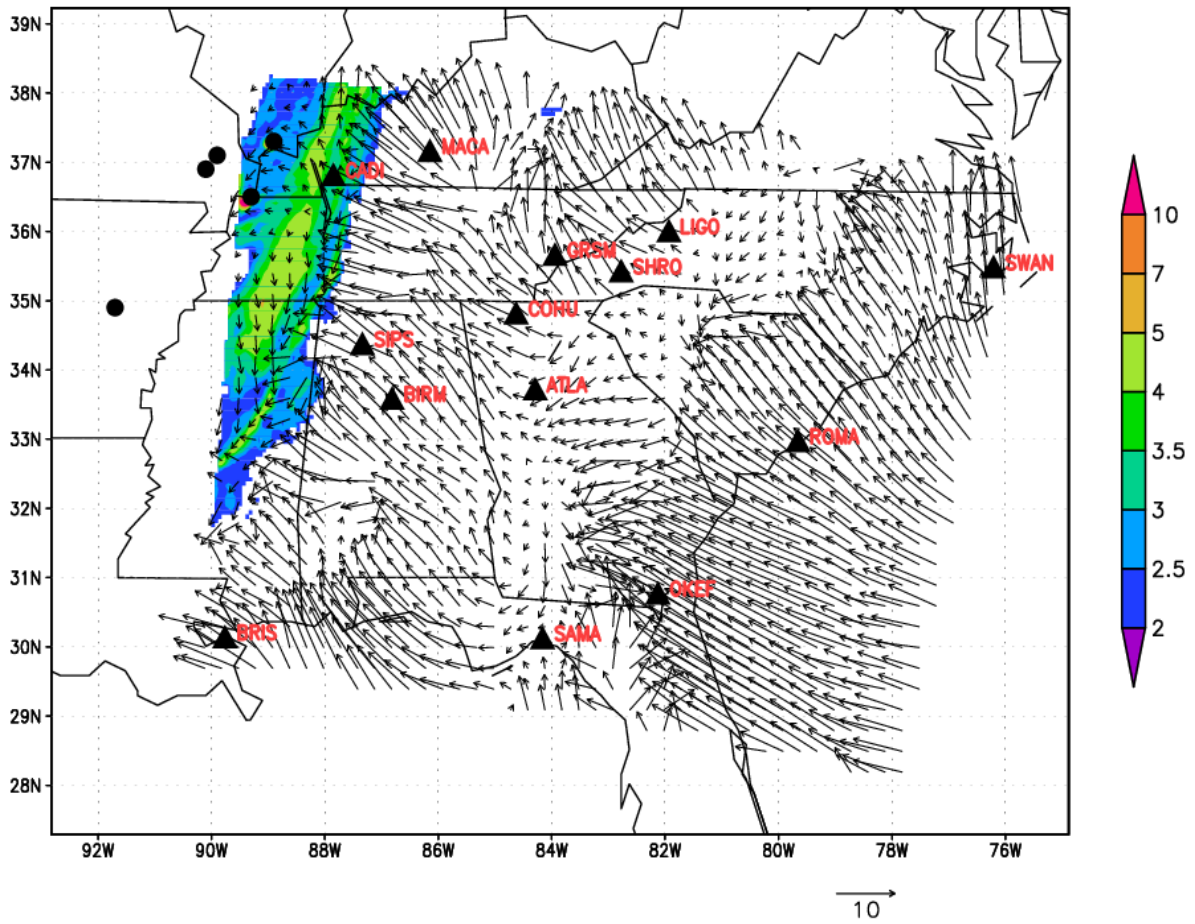
Figure 9a: same as Figure 4 but for July 03 2013.

612

613

614

615

616

617
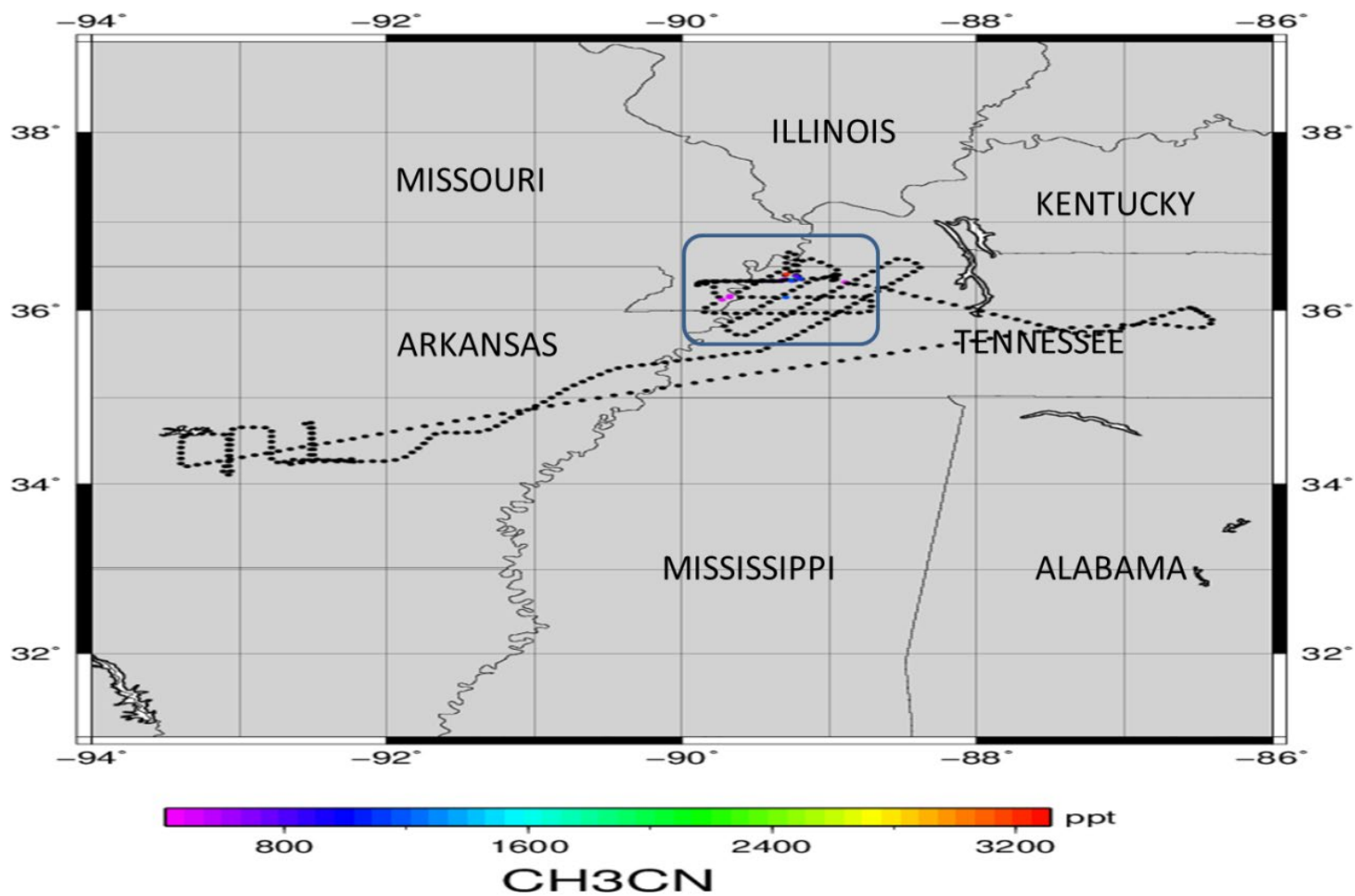
Figure 9b: the flight path of SENEX #0703 traversed the Central Plain between local time 10:00pm and 11:00pm on July 02, 2013 --- colored by measured CH3CN concentration (ppt).

620

621
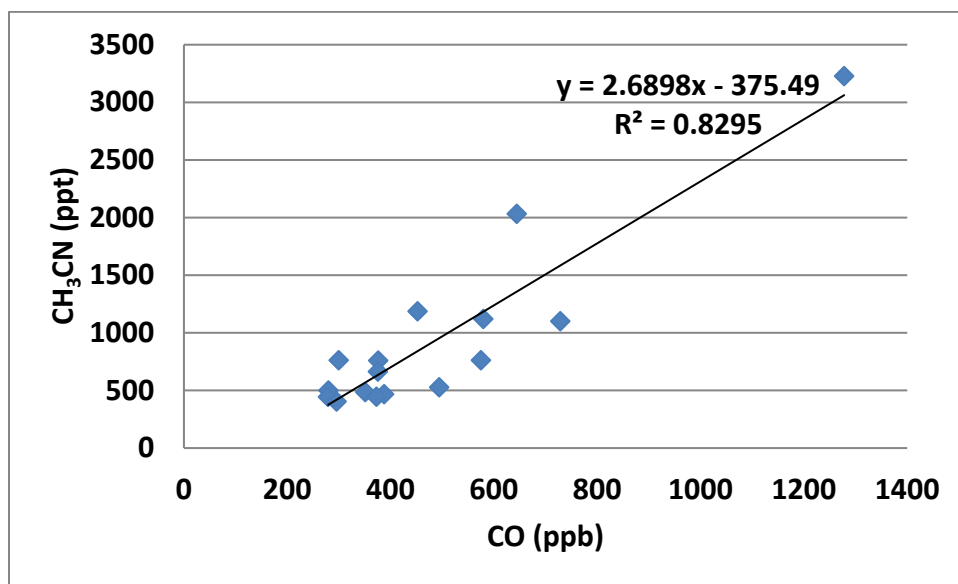
Figure 9c: CH$_3$CN (ppt) vs CO (ppb) scatter plot.

622

623
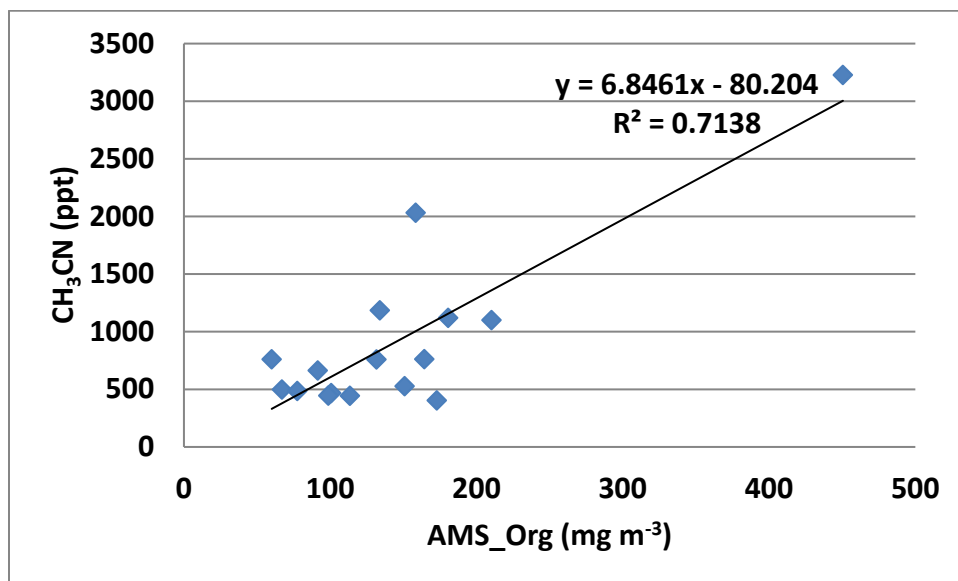
624   **Figure 9d: CH$_3$CN (ppt) vs AMS_Org (mg m^{-3}) scatter plot.**

625

38
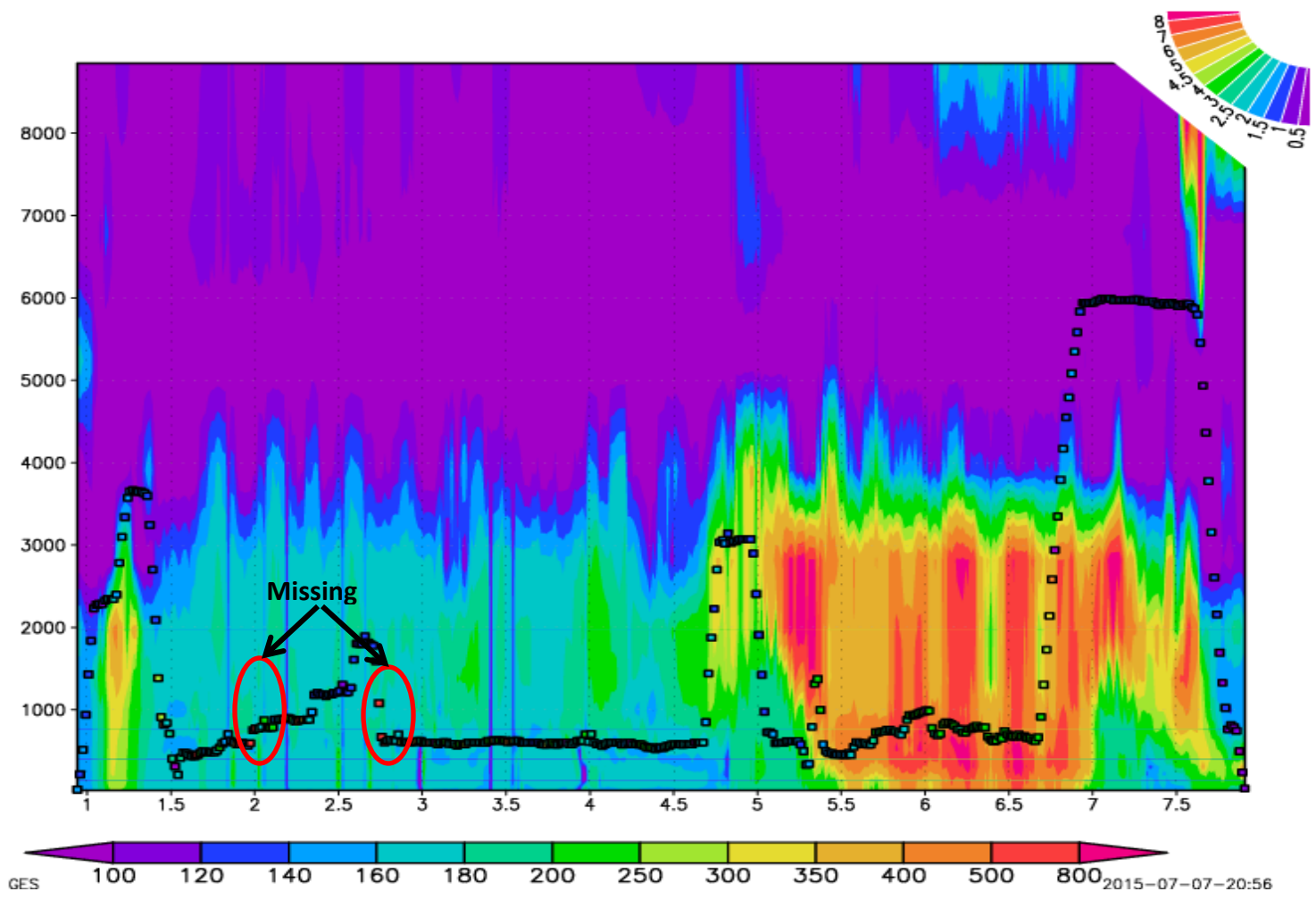
Figure 9e: same as Figure 8a but for July 03 2013. The emboldened red ovals highlight missing CH₃CN concentration measurements.

629
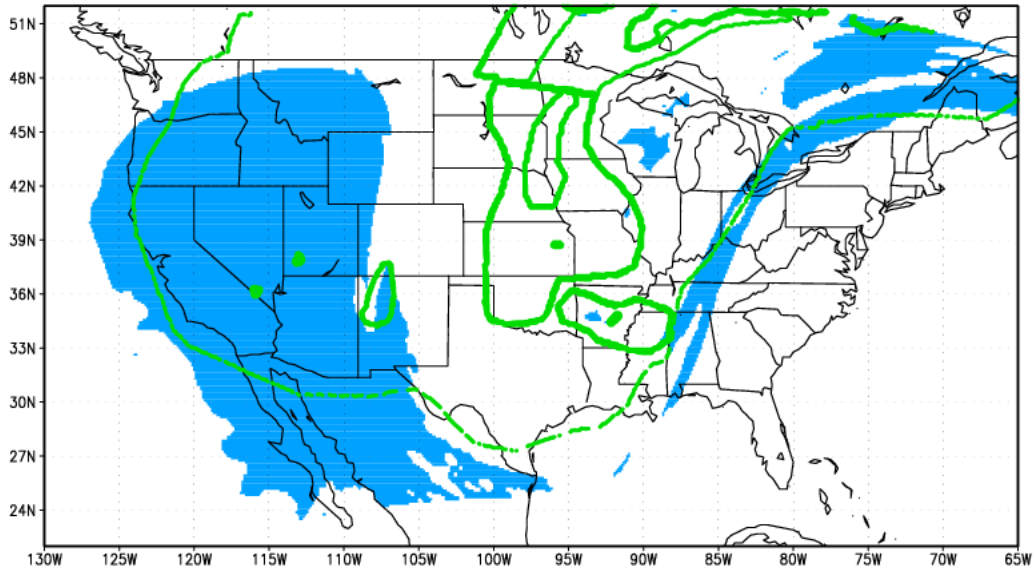
Figure 9f: same as Figure 6a but for July 03 2013.
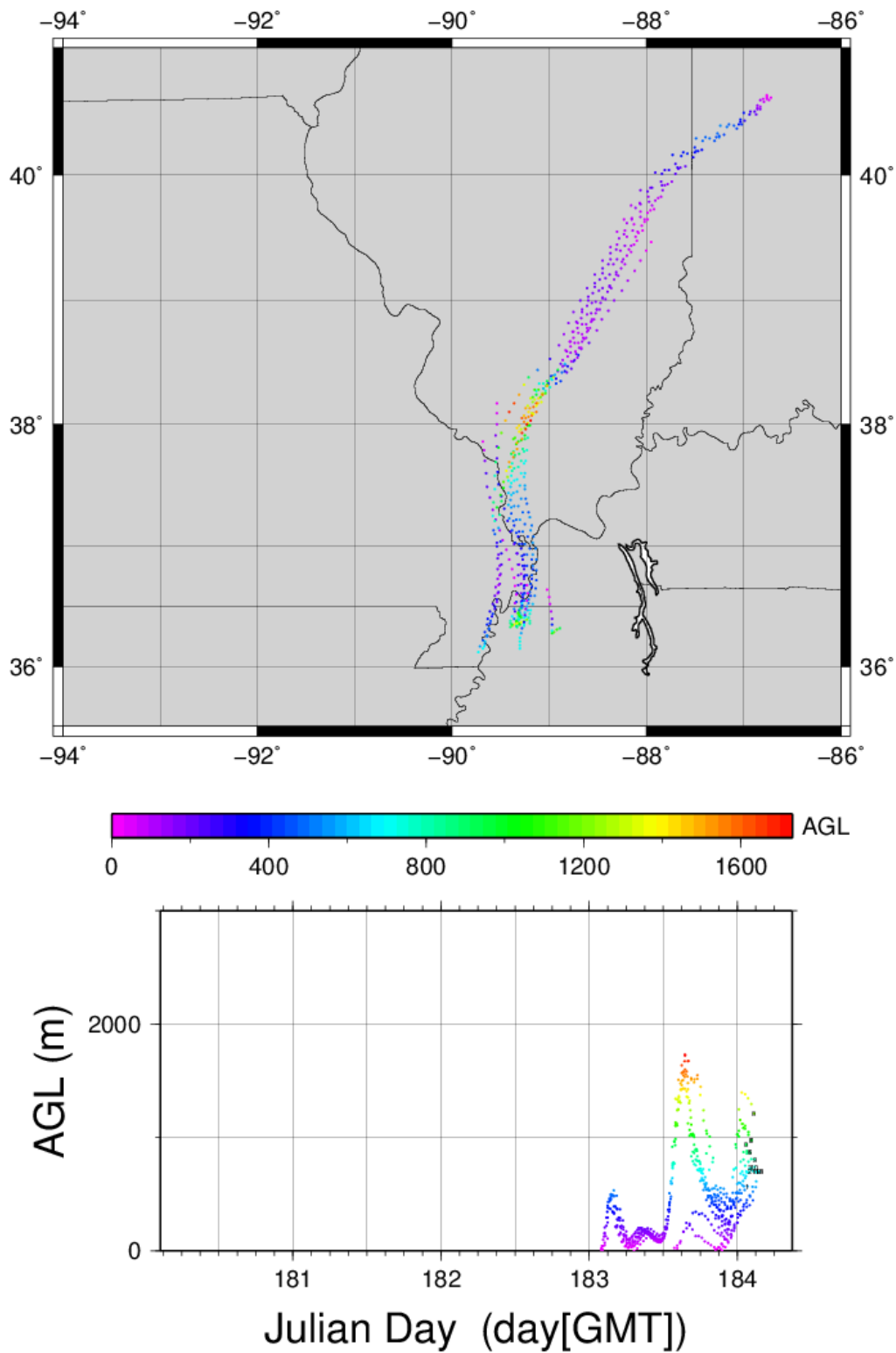
631

632

633

Figure 10: a backward trajectory analysis for CH$_3$CN concentration greater than 400 ppt measured along a SENEX flight on July 03 in: (upper) aerial, and (lower) time vertical cross-sections.

636
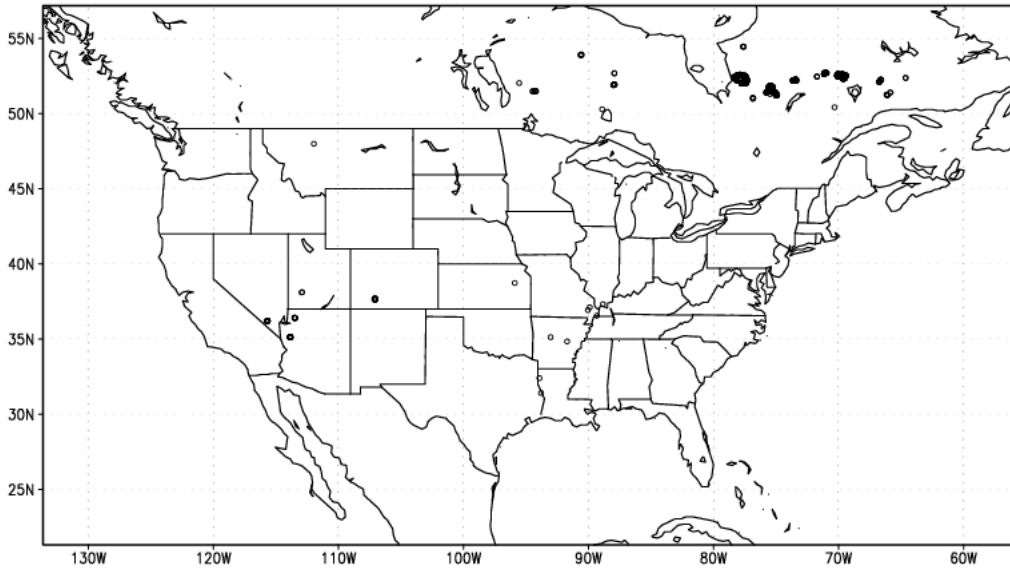
Figure 11a: fire hotspots in hmxhysplit.txt on July 03 2013 as daily composite.

638
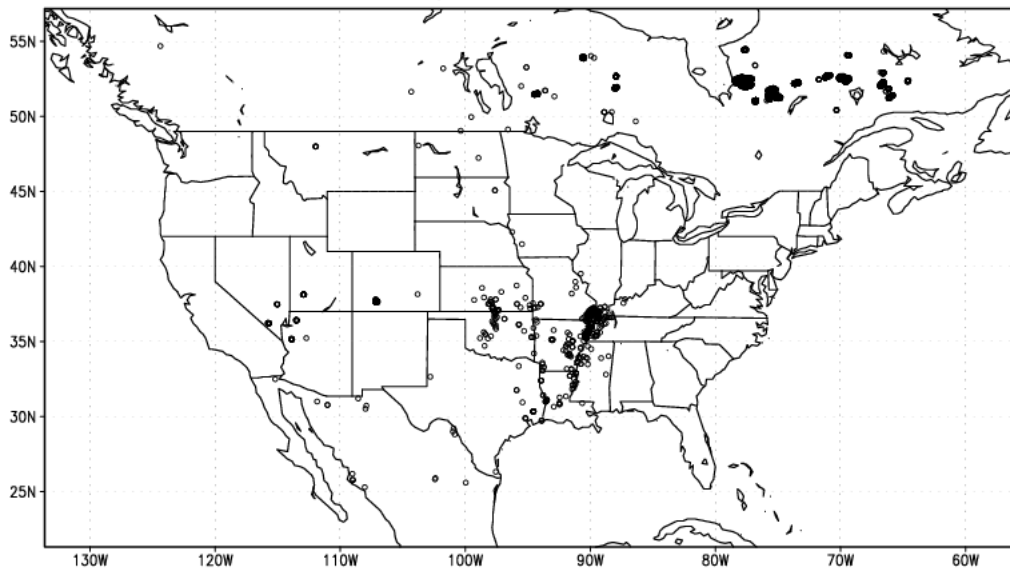
Figure 11b: fire hotspots in hmx.txt on July 03 2013 as daily composite.

640

641

642

643

644

Tables:

Table 1: observed and simulated CO (ppb) during NOAA SENEX

AGL (m)	SAMPLE SIZE	OBS	OBS_MAX	Mod_withfire	Mod_nofire	ΔCO
<500	166	128.93±38.51	319.55	108.70±21.37	107.16±20.34	1.54
500~1000	3565	146.19±44.39	1277.97	108.39±19.82	106.50±18.86	1.88
1000~1500	793	125.41±28.09	299.64	100.11±15.63	98.49±14.67	1.62
1500~2000	306	119.68±23.99	265.29	100.75±17.04	99.08±15.89	1.67
2000~2500	219	111.48±19.98	286.22	99.88±17.95	98.37±16.92	1.51
2500~3000	209	111.84±19.79	295.79	97.43±12.21	95.87±11.15	1.56
3000~3500	181	109.31±16.66	197.94	89.34±12.09	88.13±11.06	1.21
3500~4000	195	110.78±14.36	140.42	92.11±10.73	90.25±9.62	1.86
4000~5000	369	89.82±19.09	138.04	80.36±10.15	79.17±9.14	1.19
5000~6000	354	102.26±22.37	209.20	78.12±7.64	76.82±6.28	1.30
6000~7000	85	87.53±17.88	115.32	73.35±4.71	70.58±2.45	2.77

Table 2: identified fire signals from IMPROVE measurements during SENEX

Site	Date	Concentrations (ug m^{-3})						Ratio (Concentration/Average)						Ratio	
		EC	OC	K	SOIL	NO_3^-	SO_4^{2-}	EC	OC	K	SOIL	NO_3^-	SO_4^{2-}	BC/OC	K/BC
COHU	0621	0.28	2.10	0.05	0.22	0.13	2.61	1.4	1.46	1.42	0.39	0.84	1.28	0.1331	0.1933
MACA	0624	0.45	2.34	0.09	0.26	0.24	2.76	1.85	1.58	1.82	0.48	1.19	1.24	0.1929	0.1973
MACA	0703	0.33	2.32	0.08	0.16	0.29	2.11	1.35	1.57	1.73	0.29	1.43	0.94	0.1423	0.2554
BRIS	0703	0.24	0.98	0.21	0.31	0.11	2.63	1.49	1.28	2.79	0.13	0.35	1.36	0.2458	0.8851
GRSM	0621	0.25	1.56	0.05	0.24	0.13	2.52	1.36	1.45	1.24	0.49	0.99	1.42	0.1596	0.1979

Notes: (ratios for EC, OC and K > 1.2) **U** (ratio for SOIL < 1.0) **U** (ratios for NO_3^- and SO_4^{2-} < 1.5);

References:

Achtemeier, G. L., S. A. Goodrick, Y. Q. Liu, F. Garcia-Menendez, Y. T. Hu, and M. T. Odman. Modeling Smoke Plume-Rise and Dispersion from Southern United States Prescribed Burns with Daysmoke, *Atmosphere*, 2: 358-88. doi:10.3390/atmos2030358, 2011.

Aiken, A. C., B. de Foy, C. Wiedinmyer, P. F. DeCarlo, I. M. Ulbrich, M. N. Wehrli, S. Szidat, A. S. H. Prevot, J. Noda, L. Wacker, R. Volkamer, E. Fortner, J. Wang, A. Laskin, V. Shutthanandan, J. Zheng, R. Zhang, G. Paredes-Miranda, W. P. Arnott, L. T. Molina, G. Sosa, X. Querol, and J. L. Jimenez. Mexico city aerosol analysis during MILAGRO using high resolution aerosol mass spectrometry at the urban supersite (T0) - Part 2: Analysis of the biomass burning contribution and the non-fossil carbon fraction, *Atmospheric Chemistry and Physics*, 10: 5315-41. doi:10.5194/acp-10-5315-2010, 2010.

Alvarado, M. J., C. R. Lonsdale, R. J. Yokelson, S. K. Akagi, H. Coe, J. S. Craven, E. V. Fischer, G. R. McMeeking, J. H. Seinfeld, T. Soni, J. W. Taylor, D. R. Weise, and C. E. Wold. Investigating the links between ozone and organic aerosol chemistry in a biomass burning plume from a prescribed fire in California chaparral, *Atmospheric Chemistry and Physics*, 15: 6667-88. doi:10.5194/acp-15-6667-2015, 2015.

Baker, K. R., M. C. Woody, G. S. Tonnesen, W. Hutzell, H. O. T. Pye, M. R. Beaver, G. Pouliot, and T. Pierce. Contribution of regional-scale fire events to ozone and PM2.5 air quality estimated by photochemical modeling approaches, *Atmospheric Environment*, 140: 539-54. doi:10.1016/j.atmosenv.2016.06.032, 2016.

Carlton, A. G., P. V. Bhave, S. L. Napelenok, E. D. Edney, G. Sarwar, R. W. Pinder, G. A. Pouliot, and M. Houyoux. Model Representation of Secondary Organic Aerosol in CMAQv4.7, *Environmental Science & Technology*, 44: 8553-60. doi:10.1021/es100636q, 2010.

Chai, T., H. C. Kim, P. Lee, D. Tong, L. Pan, Y. Tang, J. Huang, J. McQueen, M. Tsidulko, and I. Stajner. Evaluation of the United States National Air Quality Forecast Capability experimental real-time predictions in 2010 using Air Quality System ozone and NO2 measurements, *Geoscientific Model Development*, 6: 1831-50. doi:10.5194/gmd-6-1831-2013, 2013.

Davis, A. Y., R. Ottmar, Y. Q. Liu, S. Goodrick, G. Achtemeier, B. Gullett, J. Aurell, W. Stevens, R. Greenwald, Y. T. Hu, A. Russell, J. K. Hiers, and M. T. Odman. Fire emission uncertainties and their effect on smoke dispersion predictions: a case study at Eglin Air Force Base, Florida, USA, *International Journal of Wildland Fire*, 24: 276-85. doi:10.1071/wf13071, 2015.

de Gouw, J. A., C. Warneke, D. D. Parrish, J. S. Holloway, M. Trainer, and F. C. Fehsenfeld. Emission sources and ocean uptake of acetonitrile (CH3CN) in the atmosphere, *Journal of Geophysical Research-Atmospheres*, 108. doi:10.1029/2002jd002897, 2003.

DeBell, L. J., R. W. Talbot, J. E. Dibb, J. W. Munger, E. V. Fischer, and S. E. Frolking. A major regional air pollution event in the northeastern United States caused by extensive forest fires in Quebec, Canada, *Journal of Geophysical Research-Atmospheres*, 109. doi:10.1029/2004jd004840, 2004.

Delfino, R. J., S. Brummel, J. Wu, H. Stern, B. Ostro, M. Lipsett, A. Winer, D. H. Street, L. Zhang, T. Tjoa, and D. L. Gillen. The relationship of respiratory and cardiovascular hospital admissions to the southern California wildfires of 2003, *Occupational and Environmental Medicine*, 66: 189-97. doi:10.1136/oem.2008.041376, 2009.

Draxler, R. R., and G. D. Hess. An overview of the HYSPLIT_4 modelling system for trajectories, dispersion and deposition, *Australian Meteorological Magazine*, 47: 295-308. 1998.

Dreessen, J., J. Sullivan, and R. Delgado. Observations and impacts of transported Canadian wildfire smoke on ozone and aerosol air quality in the Maryland region on June 9-12, 2015, *Journal of the Air & Waste Management Association*, 66: 842-62. doi:10.1080/10962247.2016.1161674, 2016.

707 Drury, S. A., N. Larkin, T. T. Strand, S. M. Huang, S. J. Strenfel, E. M. Banwell, T. E. O'Brien, and S. M.
708 Raffuse. INTERCOMPARISON OF FIRE SIZE, FUEL LOADING, FUEL CONSUMPTION, AND SMOKE
709 EMISSIONS ESTIMATES ON THE 2006 TRIPOD FIRE,WASHINGTON, USA, *Fire Ecology*, 10: 56-83.
710 doi:10.4996/fireecology.1001056, 2014.
711 Eatough, D. J., D. A. Eatough, L. Lewis, and E. A. Lewis. Fine particulate chemical composition and light
712 extinction at Canyonlands National Park using organic particulate material concentrations
713 obtained with a multisystem, multichannel diffusion denuder sampler, *Journal of Geophysical*
714 *Research-Atmospheres*, 101: 19515-31. doi:10.1029/95jd01385, 1996.
715 Erbrink, H. J. PLUME RISE IN DIFFERENT ATMOSPHERES - A PRACTICAL SCHEME AND SOME
716 COMPARISONS WITH LIDAR MEASUREMENTS, *Atmospheric Environment*, 28: 3625-36.
717 doi:10.1016/1352-2310(94)00197-s, 1994.
718 Giglio, L., J. Descloitres, C. O. Justice, and Y. J. Kaufman. An enhanced contextual fire detection algorithm
719 for MODIS, *Remote Sensing of Environment*, 87: 273-82. doi:10.1016/s0034-4257(03)00184-6,
720 2003.
721 Hamm, S., and P. Warneck. THE INTERHEMISPHERIC DISTRIBUTION AND THE BUDGET OF ACETONITRILE
722 IN THE TROPOSPHERE, *Journal of Geophysical Research-Atmospheres*, 95: 20593-606.
723 doi:10.1029/JD095iD12p20593, 1990.
724 Hardy, C. C., and C. E. Hardy. Fire danger rating in the United States of America: an evolution since 1916,
725 *International Journal of Wildland Fire*, 16: 217-31. doi:10.1071/wf06076, 2007.
726 Herron-Thorpe, F. L., G. H. Mount, L. K. Emmons, B. K. Lamb, D. A. Jaffe, N. L. Wigder, S. H. Chung, R.
727 Zhang, M. D. Woelfle, and J. K. Vaughan. Air quality simulations of wildfires in the Pacific
728 Northwest evaluated with surface and satellite observations during the summers of 2007 and
729 2008, *Atmospheric Chemistry and Physics*, 14: 12533-51. doi:10.5194/acp-14-12533-2014, 2014.
730 Holzinger, R., C. Warneke, A. Hansel, A. Jordan, W. Lindinger, D. H. Scharffe, G. Schade, and P. J. Crutzen.
731 Biomass burning as a source of formaldehyde, acetaldehyde, methanol, acetone, acetonitrile,
732 and hydrogen cyanide, *Geophysical Research Letters*, 26: 1161-64. doi:10.1029/1999gl900156,
733 1999.
734 Hu, X. F., C. Yu, D. Tian, M. Ruminski, K. Robertson, L. A. Waller, and Y. Liu. Comparison of the Hazard
735 Mapping System (HMS) fire product to ground-based fire records in Georgia, USA, *Journal of*
736 *Geophysical Research-Atmospheres*, 121: 2901-10. doi:10.1002/2015jd024448, 2016.
737 Huang, J., J. McQueen, J. Wilczak, I. Djalalova, I. Stajner, P. Shafran, D. Allured, P. Lee, L. Pan, D. Tong, H.
738 Huang, G. DiMego, S. Upadhayay, and L. Monache. Improving NOAA NAQFC PM2.5 predictions
739 with a bias correction approach, *Wea. Forecasting*. doi:10.1175/WAF-D-16-0118.1, 2017.
740 Jaffe, D. A., N. Wigder, N. Downey, G. Pfister, A. Boynard, and S. B. Reid. Impact of Wildfires on Ozone
741 Exceptional Events in the Western US, *Environmental Science & Technology*, 47: 11065-72.
742 doi:10.1021/es402164f, 2013.
743 Johnston, F. H., S. B. Henderson, Y. Chen, J. T. Randerson, M. Marlier, R. S. DeFries, P. Kinney, Dmjs
744 Bowman, and M. Brauer. Estimated Global Mortality Attributable to Smoke from Landscape
745 Fires, *Environmental Health Perspectives*, 120: 695-701. doi:10.1289/ehp.1104422, 2012.
746 Justice, C. O., L. Giglio, S. Korontzi, J. Owens, J. T. Morisette, D. Roy, J. Descloitres, S. Alleaume, F.
747 Petitcolin, and Y. Kaufman. The MODIS fire products, *Remote Sensing of Environment*, 83: 244-
748 62. doi:10.1016/s0034-4257(02)00076-7, 2002.
749 Knorr, W., V. Lehsten, and A. Arneth. Determinants and predictability of global wildfire emissions,
750 *Atmospheric Chemistry and Physics*, 12: 6845-61. doi:10.5194/acp-12-6845-2012, 2012.
751 Larkin, N. K., S. M. O'Neill, R. Solomon, S. Raffuse, T. Strand, D. C. Sullivan, C. Krull, M. Rorig, J. L.
752 Peterson, and S. A. Ferguson. The BlueSky smoke modeling framework, *International Journal of*
753 *Wildland Fire*, 18: 906-20. doi:10.1071/wf07086, 2009.

754   Lee, Pius, Jeffery McQueen, Ivanka Stajner, Jianping Huang, Li Pan, Daniel Tong, Hyuncheol Kim, Youhua
755   Tang, Shobha Kondragunta, and Mark Ruminski. NAQFC developmental forecast guidance for
756   fine particulate matter (PM2. 5), *Weather and Forecasting*, 32: 343-60. doi:10.1175/waf-d-15-
757   0163.1, 2017.
758   Li, Z., S. Nadon, and J. Cihlar. Satellite-based detection of Canadian boreal forest fires: development and
759   application of the algorithm, *International Journal of Remote Sensing*, 21: 3057-69.
760   doi:10.1080/01431160050144956, 2000.
761   Malm, W. C., B. A. Schichtel, M. L. Pitchford, L. L. Ashbaugh, and R. A. Eldred. Spatial and monthly trends
762   in speciated fine particle concentration in the United States, *Journal of Geophysical Research-*
763   *Atmospheres*, 109. doi:10.1029/2003jd003739, 2004.
764   Neuman, J. A., M. Trainer, S. S. Brown, K. E. Min, J. B. Nowak, D. D. Parrish, J. Peischl, I. B. Pollack, J. M.
765   Roberts, T. B. Ryerson, and P. R. Veres. HONO emission and production determined from
766   airborne measurements over the Southeast US, *Journal of Geophysical Research-Atmospheres*,
767   121: 9237-50. doi:10.1002/2016jd025197, 2016.
768   Pan, L., D. Tong, P. Lee, H. C. Kim, and T. F. Chai. Assessment of NOx and O-3 forecasting performances
769   in the US National Air Quality Forecasting Capability before and after the 2012 major emissions
770   updates, *Atmospheric Environment*, 95: 610-19. doi:10.1016/j.atmosenv.2014.06.020, 2014.
771   Pavlovic, R., J. Chen, K. Anderson, M. D. Moran, P. A. Beaulieu, D. Davignon, and S. Cousineau. The
772   FireWork air quality forecast system with near-real-time biomass burning emissions: Recent
773   developments and evaluation of performance for the 2015 North American wildfire season,
774   *Journal of the Air & Waste Management Association*, 66: 819-41.
775   doi:10.1080/10962247.2016.1158214, 2016.
776   Prados, A. I., S. Kondragunta, P. Ciren, and K. R. Knapp. GOES Aerosol/Smoke product (GASP) over North
777   America: Comparisons to AERONET and MODIS observations, *Journal of Geophysical Research-*
778   *Atmospheres*, 112. doi:10.1029/2006jd007968, 2007.
779   Prins, E. M., and W. P. Menzel. GEOSTATIONARY SATELLITE DETECTION OF BIOMASS BURNING IN
780   SOUTH-AMERICA, *International Journal of Remote Sensing*, 13: 2783-99. 1992.
781   Rappold, A. G., S. L. Stone, W. E. Cascio, L. M. Neas, V. J. Kilaru, M. S. Carraway, J. J. Szykman, A. Ising, W.
782   E. Cleve, J. T. Meredith, H. Vaughan-Batten, L. Deyneka, and R. B. Devlin. Peat Bog Wildfire
783   Smoke Exposure in Rural North Carolina Is Associated with Cardiopulmonary Emergency
784   Department Visits Assessed through Syndromic Surveillance, *Environmental Health Perspectives*,
785   119: 1415-20. doi:10.1289/ehp.1003206, 2011.
786   Reid, J. S., R. Koppmann, T. F. Eck, and D. P. Eleuterio. A review of biomass burning emissions part II:
787   intensive physical properties of biomass burning particles, *Atmospheric Chemistry and Physics*,
788   5: 799-825. 2005.
789   Rolph, G. D., R. R. Draxler, A. F. Stein, A. Taylor, M. G. Ruminski, S. Kondragunta, J. Zeng, H. C. Huang, G.
790   Manikin, J. T. McQueen, and P. M. Davidson. Description and Verification of the NOAA Smoke
791   Forecasting System: The 2007 Fire Season, *Weather and Forecasting*, 24: 361-78.
792   doi:10.1175/2008waf2222165.1, 2009.
793   Ruminski, M., and S. Kondragunta. Monitoring fire and smoke emissions with the hazard mapping
794   system - art. no. 64120B. in F. Kogan, S. Habib, V. S. Hegde and M. Matsuoka (eds.), *Disaster*
795   *Forewarning Diagnostic Methods and Management*. 2006.
796   Ruminski, M., J. Simko, J. Kibler, S. Kondragunta, R. Draxler, P. Davidson, and P. Li. Use of multiple
797   satellite sensors in NOAA's operational near real-time fire and smoke detection and
798   characterization program. in W. M. Hao (ed.), *Remote Sensing of Fire: Science and Application*.
799   2008.
800   Saide, P. E., D. A. Peterson, A. da Silva, B. Anderson, L. D. Ziemba, G. Diskin, G. Sachse, J. Hair, C. Butler,
801   M. Fenn, J. L. Jimenez, P. Campuzano-Jost, A. E. Perring, J. P. Schwarz, M. Z. Markovic, P. Russell,

802   J. Redemann, Y. Shinozuka, D. G. Streets, F. Yan, J. Dibb, R. Yokelson, O. B. Toon, E. Hyer, and G.
803   R. Carmichael. Revealing important nocturnal and day-to-day variations in fire smoke emissions
804   through a multiplatform inversion, *Geophysical Research Letters*, 42: 3609-18.
805   doi:10.1002/2015gl063737, 2015.
806   Sandberg, D.V., and J. Peterson. A source strength model for prescribed fires in coniferous logging slash,
807   *1984 annual meeting, Air Pollution Control Association, Northwest Section. 14p*. 1984.
808   Sapkota, A., J. M. Symons, J. Kleissl, L. Wang, M. B. Parlange, J. Ondov, P. N. Breysse, G. B. Diette, P. A.
809   Eggleston, and T. J. Buckley. Impact of the 2002 Canadian forest fires on particulate matter air
810   quality in Baltimore City, *Environmental Science & Technology*, 39: 24-32.
811   doi:10.1021/es035311z, 2005.
812   Schroeder, W., M. Ruminski, I. Csiszar, L. Giglio, E. Prins, C. Schmidt, and J. Morisette. Validation analyses
813   of an operational fire monitoring product: The Hazard Mapping System, *International Journal of*
814   *Remote Sensing*, 29: 6059-66. doi:10.1080/01431160802235845, 2008.
815   Singh, H. B., C. Cai, A. Kaduwela, A. Weinheimer, and A. Wisthaler. Interactions of fire emissions and
816   urban pollution over California: Ozone formation and air quality simulations, *Atmospheric*
817   *Environment*, 56: 45-51. doi:10.1016/j.atmosenv.2012.03.046, 2012.
818   Singh, H. B., L. Salas, D. Herlth, R. Kolyer, E. Czech, W. Viezee, Q. Li, D. J. Jacob, D. Blake, G. Sachse, C. N.
819   Harward, H. Fuelberg, C. M. Kiley, Y. Zhao, and Y. Kondo. In situ measurements of HCN and
820   CH3CN over the Pacific Ocean: Sources, sinks, and budgets, *Journal of Geophysical Research-*
821   *Atmospheres*, 108. doi:10.1029/2002jd003006, 2003.
822   Sofiev, M., T. Ermakova, and R. Vankevich. Evaluation of the smoke-injection height from wild-land fires
823   using remote-sensing data, *Atmospheric Chemistry and Physics*, 12: 1995-2006.
824   doi:10.5194/acp-12-1995-2012, 2012.
825   Strand, T. M., N. Larkin, K. J. Craig, S. Raffuse, D. Sullivan, R. Solomon, M. Rorig, N. Wheeler, and D.
826   Pryden. Analyses of BlueSky Gateway PM2.5 predictions during the 2007 southern and 2008
827   northern California fires, *Journal of Geophysical Research-Atmospheres*, 117.
828   doi:10.1029/2012jd017627, 2012.
829   Urbanski, S., V. Kovalev, A. Petkov, A. Scalise, C. Wold, and W. M. Hao. Validation of smoke plume rise
830   models using ground-based lidar. in C. M. U. Neale and A. Maltese (eds.), *Remote Sensing for*
831   *Agriculture, Ecosystems, and Hydrology Xvi*. 2014.
832   Warneke, C., M. Trainer, J. A. de Gouw, D. D. Parrish, D. W. Fahey, A. R. Ravishankara, A. M.
833   Middlebrook, C. A. Brock, J. M. Roberts, S. S. Brown, J. A. Neuman, B. M. Lerner, D. Lack, D. Law,
834   G. Hubler, I. Pollack, S. Sjostedt, T. B. Ryerson, J. B. Gilman, J. Liao, J. Holloway, J. Peischl, J. B.
835   Nowak, K. C. Aikin, K. E. Min, R. A. Washenfelder, M. G. Graus, M. Richardson, M. Z. Markovic, N.
836   L. Wagner, A. Welti, P. R. Veres, P. Edwards, J. P. Schwarz, T. Gordon, W. P. Dube, S. A. McKeen,
837   J. Brioude, R. Ahmadov, A. Bougiatioti, J. J. Lin, A. Nenes, G. M. Wolfe, T. F. Hanisco, B. H. Lee, F.
838   D. Lopez-Hilfiker, J. A. Thornton, F. N. Keutsch, J. Kaiser, J. Q. Mao, and C. D. Hatch.
839   Instrumentation and measurement strategy for the NOAA SENEX aircraft campaign as part of
840   the Southeast Atmosphere Study 2013, *Atmospheric Measurement Techniques*, 9: 3063-93.
841   doi:10.5194/amt-9-3063-2016, 2016.
842   Wiedinmyer, C., S. K. Akagi, R. J. Yokelson, L. K. Emmons, J. A. Al-Saadi, J. J. Orlando, and A. J. Soja. The
843   Fire INventory from NCAR (FINN): a high resolution global model to estimate the emissions from
844   open burning, *Geoscientific Model Development*, 4: 625-41. doi:10.5194/gmd-4-625-2011, 2011.
845   Wiedinmyer, C., B. Quayle, C. Geron, A. Belote, D. McKenzie, X. Y. Zhang, S. O'Neill, and K. K. Wynne.
846   Estimating emissions from fires in North America for air quality modeling, *Atmospheric*
847   *Environment*, 40: 3419-32. doi:10.1016/j.atmosenv.2006.02.010, 2006.
848   Wotawa, G., and M. Trainer. The influence of Canadian forest fires on pollutant concentrations in the
849   United States, *Science*, 288: 324-28. doi:10.1126/science.288.5464.324, 2000.

850   Xu, L., A. M. Middlebrook, J. Liao, J. A. de Gouw, H. Y. Guo, R. J. Weber, A. Nenes, F. D. Lopez-Hilfiker, B.
851   H. Lee, J. A. Thornton, C. A. Brock, J. A. Neuman, J. B. Nowak, I. B. Pollack, A. Welti, M. Graus, C.
852   Warneke, and N. L. Ng. Enhanced formation of isoprene-derived organic aerosol in sulfur-rich
853   power plant plumes during Southeast Nexus, *Journal of Geophysical Research-Atmospheres*,
854   121: 11137-53. doi:10.1002/2016jd025156, 2016.
855   Yarwood, G., S. Rao, M. Yocke, and G. Whitten. Updates to the Carbon Bond Chemical Mechanism:
856   CB05, *Technical Report RT-0400675 ENVIRON International Corporation Novato, CA, USA*. 2005.
857   Zhang, X. Y., S. Kondragunta, and B. Quayle. Estimation of Biomass Burned Areas Using Multiple-
858   Satellite-Observed Active Fires, *Ieee Transactions on Geoscience and Remote Sensing*, 49: 4469-
859   82. doi:10.1109/tgrs.2011.2149535, 2011.

860